

Visible Light Communications based on Color Shift  
Keying Scheme for Indoor Applications

A Thesis

submitted to the designated  
by the Assembly  
of the Department of Computer Science and Engineering  
Examination Committee

by

Georgios Megas

in partial fulfillment of the requirements for the degree of

MASTER OF SCIENCE IN DATA AND COMPUTER  
SYSTEMS ENGINEERING  
WITH SPECIALIZATION  
IN ADVANCED COMPUTER SYSTEMS

University of Ioannina

School of Engineering

Ioannina 2022

Examining Committee:

- **Yiorgos Tsiatouhas**, Professor, Department of Computer Science & Engineering, University of Ioannina (Advisor)
- **Aristides Efthymiou**, Assist. Professor, Department of Computer Science & Engineering, University of Ioannina
- **Vasileios Tenentes**, Assist. Professor, Department of Computer Science & Engineering, University of Ioannina

## DEDICATION

---

*To my parents*

## ACKNOWLEDGEMENTS

---

This dissertation was carried out at the VCAS Lab: VLSI Systems and Computer Architecture Laboratory of the University of Ioannina during the spring semester of the academic year 2021-2022. Firstly, I would like to warmly thank Professor Dr. Yiorgos Tsiatouhas for the trust, support, guidance, and the opportunity that he gave me to develop my knowledge in the field of Visible Light Communication (VLC) in an excellent academic and research environment.

I would like also to thank and express my appreciation to Assist. Professor Dr. Aristides Efthymiou for the guidance and the advice during this effort. Moreover, I would also like to say a massive thank you to the PhD candidate Mr. Yiorgos Papa-theodorou and to Dr. Yiorgos Sfikas for the selfless support and help. Finally, many thanks to Dr. Marina Plisiti and to the PhD candidate Christoforos Papaioannou for the excellent cooperation.

Finally, a big thank you to my family, my friends, and my partner Angeliki for supporting this decision and to all those people who, without necessarily realizing it, contributed to the completion of this effort.

# TABLE OF CONTENTS

---

List of Figures	iii
List of Tables	vi
List of Algorithms	vii
List of Abbreviations	viii
Abstract	ix
Εκτεταμένη Περίληψη	xi
<b>CHAPTER 1 Introduction</b>	<b>1</b>
1.1 Evolution of Wireless Communication.....	1
1.2 Visible Light Communication Approach.....	3
1.3 Theoretical Background.....	4
1.4 Modulation Formats.....	6
1.4.1 Color Shift Keying .....	6
1.4.2 On-Off Keying .....	7
1.5 Outline.....	7
<b>CHAPTER 2 The VLC Link</b>	<b>9</b>
2.1 Circuit Design.....	9
2.1.1 RGB Transmitter Circuit.....	10
2.1.2 Photodiode Receiver Circuit.....	11
2.2 Circuit Implementation.....	12
2.2.1 Transmitter Circuit Construction .....	12
2.2.2 Photodiode Receiver Circuit Construction.....	14
2.3 Waveform Generation .....	15

2.3.1	Available Solutions on Arbitrary Waveform Generators .....	15
2.3.2	FPGA: Altera DE2 Board.....	16
2.3.3	Pseudorandom binary sequence .....	16
2.3.4	Modulation format.....	19
2.3.5	Clock frequency .....	20
2.3.6	Schematic Diagram in Quartus Prime .....	21
2.4	Experimental Set-up.....	22
<b>CHAPTER 3</b>	<b>Circuit Characterization</b>	<b>26</b>
3.1	Photodiode Characterization .....	26
<b>CHAPTER 4</b>	<b>Data Retrieval at the Receiver</b>	<b>30</b>
4.1	The Data Retrieval Scheme Structure.....	31
4.2	Voltage Normalization.....	32
4.3	Quantization Error Correction.....	34
4.4	Digitization .....	35
4.5	Pattern Search .....	37
<b>CHAPTER 5</b>	<b>Results</b>	<b>39</b>
5.1	Effect of the Illuminance to SNR.....	39
5.2	BER Analysis .....	42
<b>CHAPTER 6</b>	<b>Conclusions and Future Work</b>	<b>47</b>
6.1	Conclusions .....	47
6.2	Future Work .....	48
	<b>Bibliography</b>	<b>50</b>

## LIST OF FIGURES

---

1.1	A block diagram for a VLC chain .....	4
1.2	The CIE 1931 color space chromaticity diagram with wavelengths in nanometers.....	7
1.3	The structure of the thesis .....	8
2.1	The circuit for red, green, and blue LEDs .....	10
2.2	The receiver circuit using a triple photodiode topology .....	12
2.3	(a) The designed circuit in EasyEda and (b) the PCB .....	13
2.4	(a) The PCB design which was developed with the EasyEDA and (b) the printed board before the components were added .....	14
2.5	A 7-stage LFSR based on D flip-flops and an XOR gate .....	17
2.6	The selected PRBS for each channel of the RGB transmitter which developed on the Altera DE2 Board with the Intel Quartus Prime Software.....	19
2.7	Manchester encoding scheme based on an exclusive OR gate .....	20
2.8	The clock frequency implementation in the Altera DE2 Board.....	21
2.9	The PRBS implementation for the three channels in the Altera DE2 Board.....	22
2.10	Block diagram of the VLC link .....	22
2.11	The experimental set-up used in the measurements.....	23
2.12	The (a) frontage and the (b) backside of the LED RGB transmitter implementation .....	24
2.13	The photodiode receiver implementation.....	25

3.1	The cross-channel interference to received signal from the photodiode. Note that, a single RGB LED is used in the transmitter of this link.....	27
3.2	The output photocurrent for illuminance of (a) 1943 lx and (b) 840 lx without the presence of the $R_{LED}$ resistors discussed in Chapter 2.....	28
3.3	The effect of the distance over the measured photocurrent.....	28
3.4	The output photocurrent for illuminance of 1943 lx at 4000 K RGB LED operation .....	29
3.5	The output photocurrent for illuminance of 1943 lx at 4000 K RGB LED operation for the eight possible states.....	29
4.1	Flowchart of the data retrieve scheme .....	31
4.2	The elbow point for the red channel .....	33
4.3	The elbow point for the green channel .....	33
4.4	The elbow point for the blue channel .....	34
4.5	The matrix which contains the length of consecutive identical samples .....	34
4.6	Retrieved samples from the PD channels for every half period .....	35
4.7	Euclidean distance between the received color $c$ and the eight different possible states .....	36
4.8	Block diagram of the Pattern Search stage for the first attempt to retrieve the PRBS pattern .....	38
4.9	Block diagram of the Pattern Search stage for the alternative method to retrieve the PRBS pattern .....	38
5.1	Gaussian distribution of noise energy.....	40
5.2	Curves of SNR versus illuminance for signal frequency 1.25 kHz.....	41
5.3	Curves of SNR versus illuminance for signal frequency 5 kHz .....	42
5.4	Curves of SNR versus illuminance for signal frequency 20 kHz .....	42
5.5	Curves of SNR versus BER for signal frequency 1.25 kHz.....	43
5.6	Curves of SNR versus BER for signal frequency 5 kHz .....	43
5.7	Curves of SNR versus BER for signal frequency 20 kHz .....	44
5.8	A 1.25 kHz received signal.....	44

5.9	A 20 kHz received signal.....	45
5.10	Curves of illuminance versus BER for signal frequencies 1.25, 5 and 20 kHz .....	46
5.11	Curves of distance versus BER for signal frequencies 1.25, 5 and 20 kHz .....	46

## LIST OF TABLES

---

2.1	Length of sequence in bits based on the order of the PRBS.....	17
2.2	Monic polynomials based on the order of the PRBS .....	18
2.3	Manchester encoding data using XOR gate.....	20

## LIST OF ALGORITHMS

---

4.1	K-Means .....	32
-----	---------------	----

## LIST OF ABBREVIATIONS

---

AWG	Arbitrary waveform generator
BER	bit error rate
BJT	Bipolar Junction Transistor
CIE	Commission Internationale de l'Éclairage
CSK	Color Shift Keying
EM	electromagnetic
FPGA	Field-programmable gate array
ITU	International Telecommunication Union
LED	light-emitting diode
LFSR	Linear-feedback shift register
LOS	Line-of-Sight
MAC	Media Access Control
NRZ	Non-return-to-zero
OOK	On-Off Keying
OWC	Optical wireless communications
PCB	printed circuit board
PD	photodiode
PRBS	Pseudo-Random Bits Stream
RF	Radio Frequency
SNR	Signal-to-noise ratio
VLC	Visible light communication
VLP	Visible light positioning
WDM	Wavelength division multiplexing
WiMax	Worldwide Interoperability for Microwave Access

## ABSTRACT

---

Georgios Megas, M.Sc. in Data and Computer Systems Engineering, Department of Computer Science and Engineering, School of Engineering, University of Ioannina, Greece, 2022.

Visible Light Communications based on Color Shift Keying Scheme for Indoor Applications.

Advisor: Yiorgos Tsiatouhas, Professor.

Over the last years Light Emitting Diodes (LEDs) have become the most popular solution in modern lighting infrastructures. Their longer lifetime and significant lower consumption are the main reasons which gave them the lead in comparison with incandescent bulbs. Moreover, LEDs due to their ability to switch on and off at high frequencies can operate as transmitters while at the same time the human-eye cannot understand this switching activity. This means that along with the illumination of the space, there is also the possibility to create new optical wireless links. The new era of lighting infrastructures created the margin for wireless communication links which are indicated as Visible Light Communication (VLC).

The new generation of wireless communications is characterized by high demands on carrier frequency, bandwidth, and of course the immunity from electromagnetic interference, areas which put the Radio Frequency (RF) spectrum under pressure. Satisfying these requirements with the present technology and infrastructure is a new technological challenge with VLC being considered as a very promising area for filling some of the technological gaps and complementing of the RF technology.

The design of a VLC link for indoor applications is a complex task which requires to take into consideration many parameters. For instance, the dimming level which

can be chosen by the user during the day, the color shift changes, and the flickering are some of the restrictions which the designer should consider. Moreover, techniques like Orthogonal Frequency Division Multiplexing (OFDM) with Wavelength Division Multiplexing (WDM) cannot be applied for the indoor applications because the above-mentioned requirements are not covered. To conclude, in order to achieve high data rates, the designer should focus not only to the modulation formats but also to hardware design of the transmitter and the receiver.

The main goal of the dissertation is the development of an optical wireless link with a RGB LED in respect with the indoor lighting standards based on the IEEE Std. 802.15.7. For this purpose, the first stage involves the design and implementation of a RGB transmitter and a photodiode receiver which will operate based on Color Shift Keying (CSK) scheme. Furthermore, three channels were developed which operate in different wavelengths in the area of red, green and blue colors i.e., around 680 nm, 510 nm and 475 nm respectively. The second stage involves the implementation of a pseudorandom binary sequence (PRBS) for On-Off Keying modulation schemes.

Approaching this topic from the receiver's side the goal is to retrieve the incoming signals from the three channels of the photodiode. Towards this direction, a software-based algorithm in Matlab<sup>®</sup> was developed for the link characterization and bit error rate (BER) calculation. Moreover, in order to achieve robustness to the whole implementation clustering algorithms like K-Means and signal processing techniques were used. Finally, in order to extract the measurements on the transmitter and the receiver a printed circuit board (PCB) was constructed.

## ΕΚΤΕΤΑΜΕΝΗ ΠΕΡΙΛΗΨΗ

---

Γεώργιος Μέγας, Δ.Μ.Σ. στη Μηχανική Δεδομένων και Υπολογιστικών Συστημάτων, Τμήμα Μηχανικών Η/Υ και Πληροφορικής, Πολυτεχνική Σχολή, Πανεπιστήμιο Ιωαννίνων, 2022.

Επικοινωνίες Ορατού Φωτός βασισμένες σε μέθοδο Colour Shift Keying για Εφαρμογές Εσωτερικού Χώρου.

Επιβλέπων: Γιώργος Τσιατούχας, Καθηγητής.

Τα τελευταία χρόνια οι Δίοδοι Εκπομπής Φωτός (LED, light-emitting diode) έχουν γίνει η πιο δημοφιλής λύση στις σύγχρονες υποδομές φωτισμού. Η μεγαλύτερη διάρκεια ζωής τους και η σημαντικά χαμηλότερη κατανάλωση είναι οι κύριοι λόγοι που τους έδωσαν το προβάδισμα σε σύγκριση με τους λαμπτήρες πυρακτώσεως. Επιπλέον, τα LED λόγω της ικανότητάς τους να ανάβουν και να σβήνουν σε υψηλές συχνότητες μπορούν να λειτουργήσουν ως πομποί ενώ ταυτόχρονα το ανθρώπινο μάτι δεν μπορεί να αντιληφθεί αυτή τη δραστηριότητα εναλλαγής κατάστασης. Αυτό σημαίνει ότι παράλληλα με τον φωτισμό του χώρου, υπάρχει και η δυνατότητα δημιουργίας νέων οπτικών ασύρματων ζεύξεων. Η νέα εποχή των υποδομών φωτισμού δημιούργησε το περιθώριο για ασύρματες συνδέσεις επικοινωνίας που είναι γνωστές ως Επικοινωνίες Ορατού Φωτός (VLC, Visible Light Communication).

Η νέα γενιά ασύρματων επικοινωνιών χαρακτηρίζεται από υψηλές απαιτήσεις στη συχνότητα του φέροντος σήματος, στο εύρος ζώνης και φυσικά την ατρωσία από ηλεκτρομαγνητικές παρεμβολές, απαιτήσεις που θέτουν υπό πίεση το φάσμα Ραδιοσυχνοτήτων (Radio Frequency - RF). Η ικανοποίηση αυτών των απαιτήσεων με την παρούσα τεχνολογία και υποδομή είναι μια νέα τεχνολογική πρόκληση με

το VLC να θεωρείται ως ένας πολλά υποσχόμενος τομέας για την κάλυψη ορισμένων τεχνολογικών κενών αλλά και ως ένα επικουρικό μέσο για την τεχνολογία RF.

Ο σχεδιασμός μιας ζεύξης VLC για εφαρμογές εσωτερικού χώρου είναι μια πολύπλοκη διαδικασία που απαιτεί να ληφθούν υπόψη πολλές παράμετροι. Για παράδειγμα, το επίπεδο έντασης το οποίο μπορεί να επιλέξει ο χρήστης κατά τη διάρκεια της ημέρας, η αλλαγή χρώματος και το τρεμόπαιγμα είναι μερικοί από τους περιορισμούς που πρέπει να λάβει υπόψη ο σχεδιαστής. Επιπλέον, τεχνικές όπως η Ορθογώνια Πολυπλεξία Διαίρεσης Συχνότητας (OFDM, Orthogonal Frequency Division Multiplexing) με Πολυπλεξία Διαίρεσης Μήκους Κύματος (WDM, Wavelength Division Multiplexing) δεν μπορούν να εξυπηρετήσουν εφαρμογές εσωτερικού χώρου επειδή δεν καλύπτονται οι προαναφερθείσες απαιτήσεις. Συμπερασματικά, για να επιτευχθούν υψηλοί ρυθμοί δεδομένων, ο σχεδιαστής θα πρέπει να επικεντρωθεί όχι μόνο στις μέθοδο διαμόρφωσης και διαχείρισης σήματος αλλά και στη σχεδίαση του κατάλληλου υλικού του πομπού και του δέκτη.

Κύριος στόχος της διπλωματικής εργασίας είναι η ανάπτυξη μιας οπτικής ασύρματης ζεύξης με LED που λειτουργούν στο ορατό φάσμα με σεβασμό των προτύπων εσωτερικού φωτισμού που βασίζονται στο IEEE Std. 802.15.7. Για το σκοπό αυτό, το πρώτο στάδιο περιλαμβάνει τη σχεδίαση και κατασκευή ενός πομπού RGB και ενός δέκτη φωτοδιόδου που θα λειτουργούν βασισμένοι στο σχήμα Color Shift Keying (CSK). Επιπλέον, θα αναπτυχθούν τρία κανάλια που θα λειτουργούν σε διαφορετικά μήκη κύματος στην περιοχή των χρωμάτων κόκκινου, πράσινου και μπλε, δηλαδή περίπου 680 nm, 510 nm και 475 nm αντίστοιχα. Το δεύτερο στάδιο περιλαμβάνει την υλοποίηση μιας Ψευδοτυχαίας Δυαδικής Ακολουθίας (pseudorandom binary sequence - PRBS) για σχήματα διαμόρφωσης βασισμένα σε On-Off Keying.

Προσεγγίζοντας το θέμα από την πλευρά του δέκτη, στόχος είναι ανακτηθούν τα εισερχόμενα σήματα που λαμβάνονται από τα τρία κανάλια της φωτοδιόδου με αντίστοιχη ευαισθησία στα χρώματα κόκκινο, πράσινο και μπλε. Για το λόγο αυτό, αναπτύχθηκε ένας αλγόριθμος στο Matlab<sup>®</sup> για τον χαρακτηρισμό ζεύξεων και τον υπολογισμό των σφαλμάτων. Επιπλέον, για να επιτευχθεί ευρωστία στο σύνολο της υλοποίησης χρησιμοποιήθηκαν αλγόριθμοι ομαδοποίησης όπως K-Means και τεχνικές επεξεργασίας σήματος. Τέλος, για να υποστηριχθούν οι μετρήσεις στον πομπό

και το δέκτη πραγματοποιήθηκε σχεδίαση και κατασκευή πλακέτας τυπωμένου κυκλώματος (PCB, Printed Circuit Board).

# CHAPTER 1

## INTRODUCTION

---

### 1.1 Evolution of Wireless Communication

### 1.2 Visible Light Communication Approach

---

## 1.1 Evolution of Wireless Communication

The history of the wireless communication started from the early days of mankind by the Chinese, Roman and Greek cultures. Optical signals with fires, flags or smoke were the first wireless communications which transmitted the information over a Line-of-Sight (LOS) distance [UCG16].

Over the years, telecommunications developed, and the approach changed with the understanding of magnetic and electric properties through the experiments which conducted in the 17th and 18th centuries. The first form of a modern telecommunication system was a wireless communication network which operated in radio waves by Heinrich Hertz in 1888 [BB4].

The above-mentioned radio waves range from 30 Hz to 30 MHz and belong to the electromagnetic spectrum. Approaching the electromagnetic spectrum through the lens of telecommunication two more areas are available for the modern wireless networks: a) the microwave or radio frequency (RF) domain and b) the Visible Light Communication (VLC) domain. In addition, the development of a RF link should be

done in compliance with the license restrictions by the International Telecommunication Union (ITU).

The emerging wireless communication technologies are dealing with the constantly increasing data traffic and as a result the management of the available bandwidth is critical. Moreover, the IoT applications have also put under pressure the telecommunication networks. Some of the most important challenges that the RF technologies are facing are listed below [UCG16]

- **Bandwidth increase within the available RF telecommunication network:** The ITU standards are constantly changing, and it is very important that the network follows the technological changes. Moreover, solutions such as completely re-allocating the RF domain are not sustainable due to the amount of the interconnected devices and the infrastructure [EMW8].
- **Better utilization of the available bandwidth:** The more efficient bandwidth utilization is an area of study which has been developed since the first generation of wireless networks. However, the last years not made significant progress is reported [HH15].
- **Increase of access points (AP):** This challenge aims to the evolution of the network infrastructure and to create smaller cells. However, the cost of such approach might not be a sustainable and a future proof solution.

The above-mentioned areas of studies pinpoint the increased popularity for implementations based on the Optical Wireless Communication (OWC). The OWC cover the visible light, infrared, and ultraviolet areas of the electromagnetic spectrum. In comparison with the RF domain, the OWC provide unlicensed bandwidth of thousands of THz. Furthermore, the immunity to the electromagnetic interference is another important advantage of the OWC because not only adds robustness to the network but also can be used along with the RF technology [UCG16].

## 1.2 Visible Light Communication Approach

Light Emitting Diodes (LEDs), and lasers are just a few examples of the many ways visible light may be produced. The LED has a longer lifetime and uses less energy than its forerunners, which has led to its widespread use in contemporary lighting infrastructures. Additionally, LEDs have a large on/off switching rate that makes it hard for the human eye to comprehend. This characteristic led to the development of a lighting system that would not only offer illumination but also communication capabilities. Today, indoor VLC applications either focuses on localization or high-speed communication [UCG16].

Visible Light Positioning (VLP), which often functions at low data rates, is described as indoor visible light localization [KV21]. The creation of VLP systems, among other things, was prompted by the Global Positioning System's (GPS) inability to function inside buildings. A VLP system was shown to be able to localize objects with a few centimeters of precision [KV21]. The RF spectrum crunch problem is the driving force behind indoor high-speed VLC, hence VLC is seen as an aiding wireless communication technique for RF. The use of VLC is not just restricted to indoor settings; literature has also documented uses for vehicles and underwater environments [KV21].

A simplified block diagram of the VLC chain is shown in Figure 1.1. Depending on the modulation method used in the "modulation signal block," digital data representing, for example, a video file, is transformed into an electrical modulation signal. Before being sent to the LED or laser that emits visible light, this electrical signal may be further conditioned. In this case, the supplied electrical signal is transformed into its matching optical power output to produce the light signal that carries information. The applied electrical signal must meet the same conditions since the optical power is real-valued and unipolar. Contrastingly, RF signals are complex and bipolar, necessitating a change of the RF modulation methods in order to make them suitable for VLC. When indoor VLC is used, the emitted light travels through the air to a visible light receiver, which is either a photodiode (PD) or imaging sensor. In order to retrieve the sent digital data, the incident light signal is transformed back into its electrical equivalent in this instance. It is then further conditioned before being passed to the "signal demodulation block."

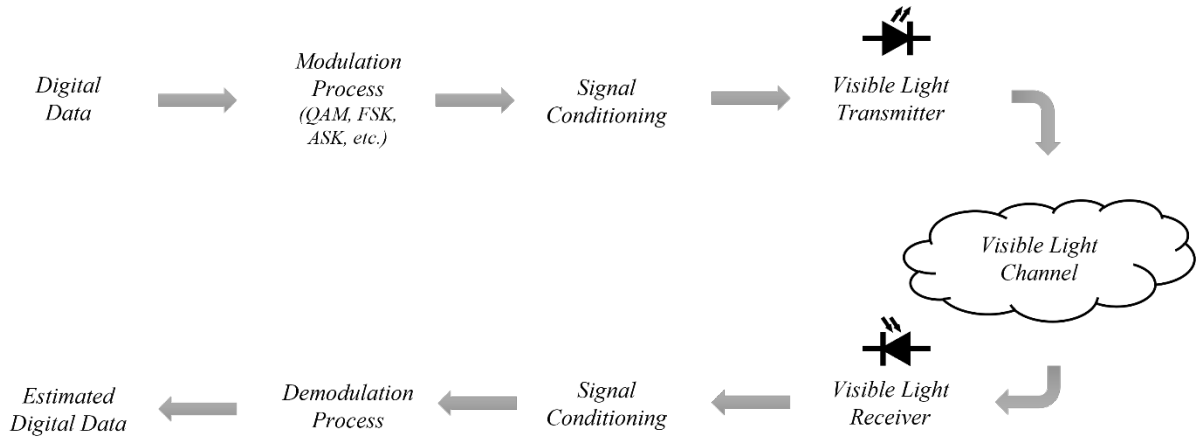


Figure 1.1: A block diagram for a VLC chain.

### 1.3 Theoretical Background

In order to understand the basic principles behind the physics of a VLC link, a brief introduction to photometry should be done. Photometry studies and measures the emission, transport and effects of light energy incident on various surfaces, and it is limited to the EM waves that stimulate our eye. In addition, the quantities it measures are weighted by the response curve of the human eye at the various frequencies. Furthermore, the measurements are based on the sensation created by the light energy in the eye.

The amount of light from a light point source or the luminous flux ( $\Phi$ ) is quotient of the light energy emitted by the source to the corresponding time weighted by the sensitivity curve of the human eye as shown in Equation 1.1.

$$\Phi = \frac{dE}{dt}, \quad (1.1)$$

and is measured in lumen (lm). In case of a monochromatic frequency radiation the Equation 1.1 is calculated by the Equation 1.2

$$\Phi = \frac{N \cdot h \cdot f}{t}, \quad (1.2)$$

where  $N$  is the number of photons and the product of  $h \cdot f$  the energy of the photon. In addition, if the light source is not monochromatic the luminous flux is given by the Equation 1.3

$$\Phi_e = \int_{\lambda_1}^{\lambda_2} \varphi_e(\lambda) d\lambda, \quad (1.3)$$

where  $\lambda$  is the wavelength and  $\varphi_e$  spectral distribution of emitted light. For a VLC link which is based on LOS it is important to know how a LED radiates in a specific direction so the solid angle must be calculated as shown in Equation 1.4

$$d\Omega = \frac{dS}{r^2} \quad (1.4)$$

where  $S$  is the spherical surface area and  $r^2$  is the radius of the considered sphere and is measured in steradian. The luminous intensity from a light point source is the quotient of the luminous flux emitted by the source in a certain direction within a solid angle  $d\Omega$  to that solid angle as shown in Equation 1.5 and is measured in candela (cd).

$$I = \frac{d\Phi}{d\Omega} \quad (1.5)$$

Approaching the VLC link from the receiver's side the surface illuminance should be calculated because the photodiode will transform the incoming photons to photocurrent. The surface illuminance at point A, is the quotient of the vertically incident luminous flux on the very small portion  $dS$  of the surface around A by the area  $dS$  is given by the Equation 1.6 and is measured in lux ( $\text{lm}/\text{m}^2$ ).

$$B = \frac{d\Phi}{dS} \quad (1.6)$$

Furthermore, for a light point source the surface illuminance is given by the Equation 1.7

$$B = \frac{I}{r^2} \cos(\varphi) \quad (1.7)$$

where the surface illuminance is inversely proportional to the square of the distance.

## 1.4 Modulation Formats

### 1.4.1 Color Shift Keying

The third physical layer realization (PHYIII), described in the VLC standard when the VLC link consists of LEDs and photodiodes is known as Color Shift Keying (CSK) [IEEEstd]. The Commission International de l'Eclairage (CIE) 1931 chromaticity diagram is used to transform data into xy color coordinates. Various studies have been carried out which proposed 4, 8, and 16-point CSK [LYW17, SK15] and there also studies based on machine learning [PW20].

Figure 1.2 shows the color space chromaticity diagram by the CIE. According to the CSK scheme the amount of possible xy color coordinates indicate the intensity of each individual LED. An optimization issue known as the set of xy color coordinates seeks to maximize the distance between the pairs of xy color coordinates that make up the set, while also taking into account the target illumination color and total optical power output [PFHM15].

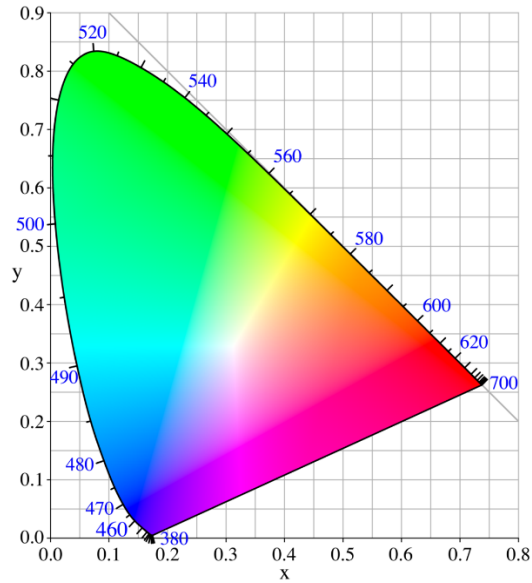


Figure 1.2: The CIE 1931 color space chromaticity diagram with wavelengths in nanometers.

### 1.4.2 On-Off Keying

On-Off Keying is the simplest form of amplitude shift keying modulation which the digital data can be presented as the absence or presence of a carrier signal. However, the design of a VLC links demands the mitigation of flickering, so an encoded process should be added. Manchester encoding is selected and analyzed in Chapter 2. As a result, the VLC standard mentions two distinct dimming techniques for OOK. To achieve the required illumination level, the first method, known as Variable OOK, adds compensation time to the data stream. The second method redefines the optical power that is released both in the on and off states [IEEEstd].

## 1.5 Outline

The structure of this thesis is shown in Figure 1.3. In Chapter 2, the implementation of the VLC link is presented including the implementation of the RGB LED transmitter along with the photodiode receiver. This chapter also deals with the implementation of the waveform generation based on a FPGA platform and the

experimental set-up. Chapter 3, presents the photodiode characterization. In Chapter 4, the data retrieval scheme at the receiver based on the Euclidean distance is presented. Finally, in Chapter 5 the experimental results are presented.

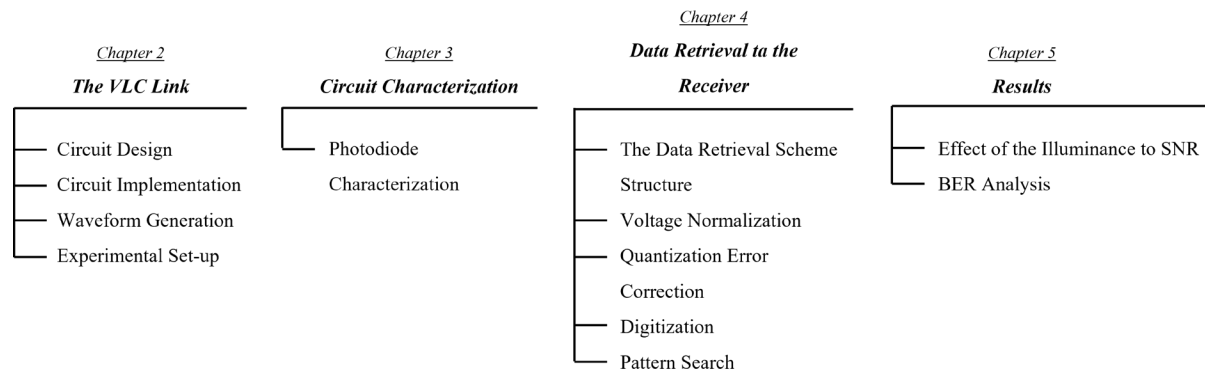


Figure 1.3: The structure of the thesis.

## CHAPTER 2

# THE VLC LINK

---

- 2.1 Circuit Design
  - 2.2 Circuit Implementation
  - 2.3 Waveform Generation
  - 2.4 Experimental Set-up
- 

This chapter is devoted to the implementation of the VLC link in order to highlight all the general idea behind this topic and to understand each element. The first section describes the circuits of both the RGB transmitter and the photodiode receiver and their adaptation for supporting VLC. In addition, for the circuit of the RGB transmitter a LED driver implementation is presented. Next the PCB circuit implementation is discussed. The third section describes the implementation of an arbitrary waveform generator (AWG) based on a field programmable gate array (FPGA) platform. Finally, in the fourth section is presented the experimental set-up and the devices that have been used are presented.

### 2.1 Circuit Design

In this section the hardware that supports this thesis is presented. Particularly, it is divided in two parts, with the first one devoted to the circuit design of the transmitter and the second dealing with the design of the receiver. Their functionality is also

presented and explained in order to fully understand the requirements of the VLC which are made based on the indoor applications.

### 2.1.1 RGB Transmitter Circuit

The RGB transmitter implementation is based on On/Off LED drivers, aiming to achieve high energy efficiency. Due to the nature of the RGB transmitter three circuits should be designed, one for each channel. Particularly, the circuits are almost identical with their only difference the value of the resistor in series with the LED. The proper selection of these resistances will determine the color temperature in the final signal. Figure 2.1 shows the designed circuit.

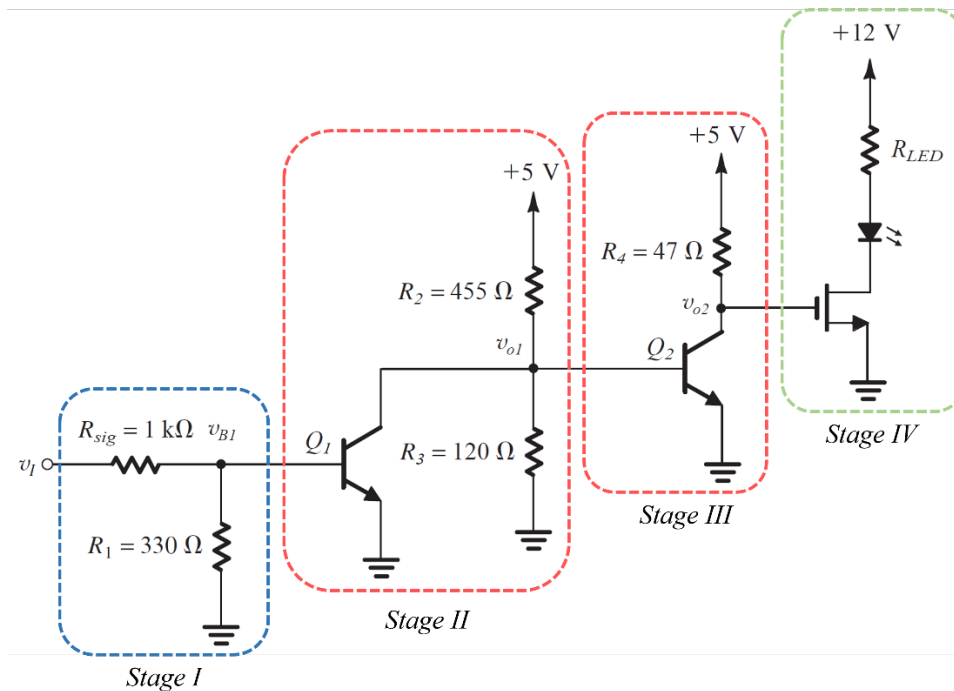


Figure 2.1: The circuit for each channel<sup>1</sup>. The  $R_{LED}$  is selected separately for the three channels in order to achieve the proper color temperature. The examined color temperature was 4000 K. The used BJTs were the Q2N2222 and the NMOS was the AO3406. Finally, the  $R_{RED, LED}$  was 42.3  $\Omega$ , the  $R_{GREEN, LED}$  was 13  $\Omega$  and the  $R_{BLUE, LED}$  was 62.6  $\Omega$ .

<sup>1</sup> The electronic circuit was a contribution of Dr. Yiorgos Sfikas, Laboratory Teaching Staff of University of Ioannina, and member of VCAS Lab.

The Stage I is a simple voltage divider, which passes a current in the order of 10 uA to the Stage II and its input is applied the transmitted signal which is an On-Off Keying pulse. The Stage II operates as a current amplifier and its output current is in the order of 1 mA. Moreover, the Stage III operates with similar way with the Stage II and the output current which is applied to the gate of NMOS is in the order of 100 mA. The final stage, Stage IV, increases the resistance to the input in order to protect the BJTs. Furthermore, in order to decrease the rising time of the pulse the  $R_4 = 47 \Omega$  was carefully selected. Finally, the Stage IV represents an approach of a series configuration LED driver.

An important stage of the transmitter implementation is the LED which operates around 12 V while the maximum forward current is 250 mA. The selected NMOS is characterized by a low on-resistance with less than 70 m $\Omega$  for  $V_{GS} = 4.5$  V which contributes to low power dissipation. Furthermore, the switching performance requirements are covered by the selected topology due to its high driving strength. Finally, the LED current is limited by the  $R_{LED}$  and can be easily calculated by the Equation 2.1.

$$I_{LED} = \frac{V_{cc} - V_{LED}}{R_{LED}} \quad (2.1)$$

### 2.1.2 Photodiode Receiver Circuit

For the receiver circuit implementation, the photodiode Kingbright APS5130PD7C-P22 was selected which consists of three channels, one channel for each color, Red, Green, and Blue in one chip.

When photons reach the photodiode, a current is generated, so in order to measure the voltage, three resistors were added, one in each channel as shown in the Figure 2.2.

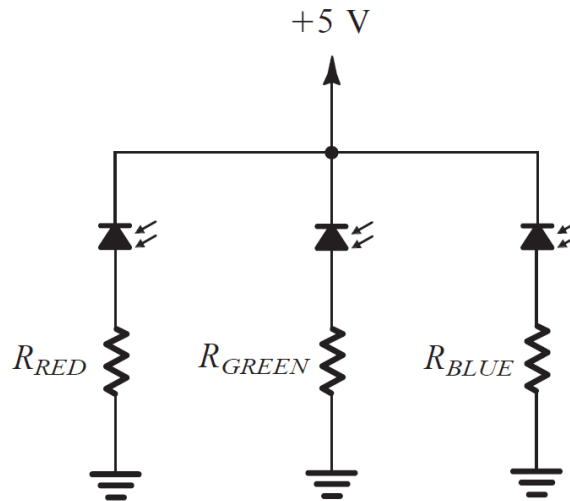


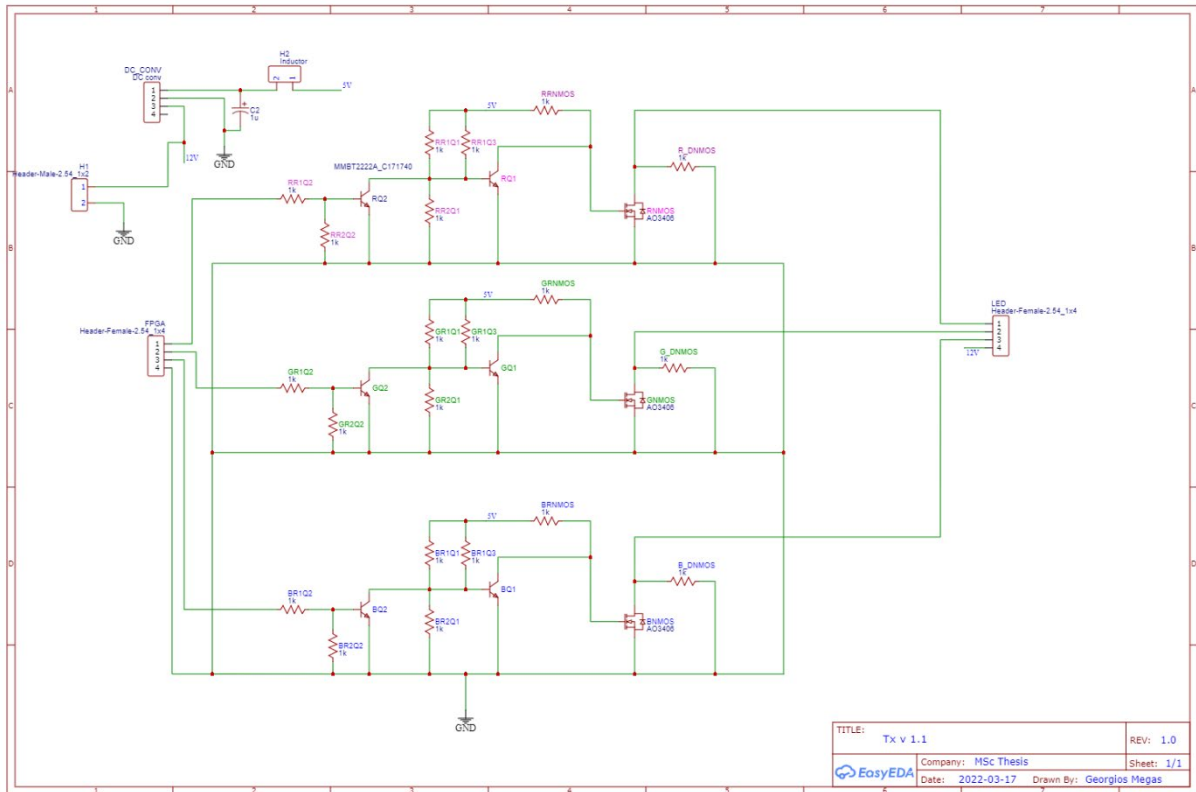
Figure 2.2: The receiver circuit using a triple photodiode topology where all photodiodes share a common cathode. The resistors  $R_{RED}$ ,  $R_{GREEN}$  and  $R_{BLUE}$  was 100 k $\Omega$ .

## 2.2 Circuit Implementation

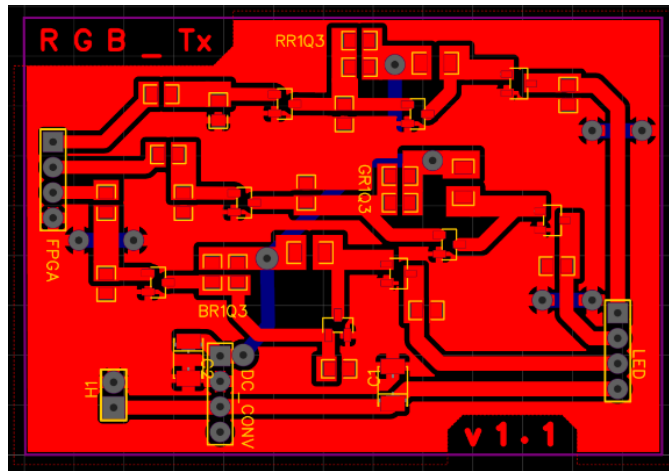
The PCB implementation of the analog circuits of the transmitter and the receiver are also areas which are covered in this thesis. Finally, technical details are presented in this section, as well as modifications and problems that occurred during the construction process.

### 2.2.1 Transmitter Circuit Construction

After the circuit design, the next crucial step was the constructions of the transmitter. Aiming to reduce noise and parasitic phenomena, to provide a miniaturized synthesis and achieve a robust circuit, a PCB implementation was decided. The first step was to design the analog circuit using the EasyEDA tool and then to extract the PCB design. The schematics are shown in Figure 2.3.



(a)



(b)

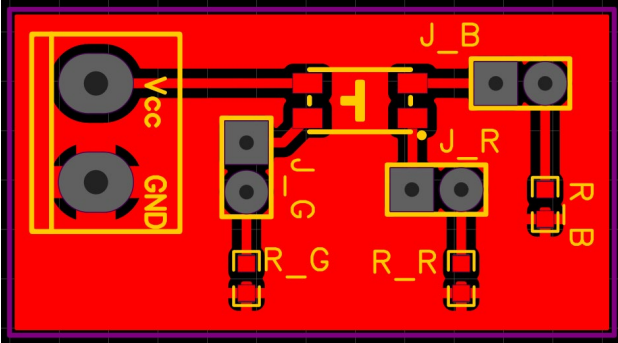
Figure 2.3: (a) The designed circuit in EasyEDA and (b) the PCB. In order to achieve the 5 V power supply, a DC converter was used. Finally, capacitors were added to operate as low pass filters

For the purposes of this thesis a single layer PCB was chosen, and the result is shown in Figure 2.3b. Furthermore, some adjustments were made to final circuit.

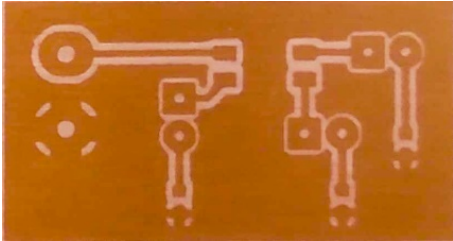
Particularly, an inductor was added in series with the C2 capacitor and with the collectors of the BJTs. To this point, it should be reminded that all the collectors of the npn BJTs are supplied with 5 V and as consequence the C1 capacitor was not needed. The capacitors are indicated in Figure 2.3a.

### 2.2.2 Photodiode Receiver Circuit Construction

The construction of the photodiode receiver circuit is a straightforward task due to its simplicity. Moreover, for each channel a 100 KΩ resistance was added. The Figure 2.4a presents the PCB design and the Figure 2.4b presents the board after the completion of the PCB process.



(a)



(b)

Figure 2.4: (a) The PCB design which was developed with the EasyEDA and (b) the printed board before the components were added.

## 2.3 Waveform Generation

The waveform generation is a very important block of the implementation of the transmitter. Particularly, the modulation format of the transmitted signal depends on the waveform generator. The proper choice of the modulation format is based on parameters such as the available bandwidth and the power efficiency which reflect the targeted VLC application demands. In this section, a brief discussion about the available commercial devices is given, followed by an implementation approach that exploits a field-programmable gate array (FPGA). The FPGA waveform generator is based on pseudorandom binary sequences which are discussed in this section.

### 2.3.1 Available Solutions on Arbitrary Waveform Generators

Nowadays, a wide variety of arbitrary waveform generators (AWG) are provided by the market, offering a great number of choices which can cover the constantly growing demands and needs. Some of the most important selection criteria include among others the available resolution, the sampling rate, the price, and the number of channels. Through bird's eye view the main selection criteria for buying an AWG might be based on the available resources and the requirements of the implementation. For instance, companies like the Keysight, Tektronix and National Instruments PXI Modules which invest on AWGs, provide products in a cost range from a few thousand Euros to hundreds of Euros.

An alternative approach to reduce cost is to use a field-programmable gate array (FPGA). Although there are two main companies in the industry the Xilinx (AMD) and the Altera (Intel), the price range is smaller compared to the AWGs. On the other hand, the developer needs to know how to operate a FPGA and to be familiar with hardware description languages while the cost ranges few hundred of Euros for our needs. Moreover, in order to minimize the cost single board computers (SBCs) like Raspberry Pi and development boards like Nucleo by STMicroelectronics can be exploited. Finally, the SBCs have shown a versatile functionality and huge processing power improvement while the cost is very low (tens of Euros).

Designing a VLC link the requirements for the waveform generation must be taken into consideration. Particularly, the sufficient sampling rate for high-speed

signals often demands tens of Mega Samples per second (MS/s) and in some cases such as real-time application the sampling rate demands increase.

### **2.3.2 FPGA: Altera DE2 Board**

Various studies for AWGs based on FPGA implementations have been proposed which have shown great capabilities in the sampling rate and the available bandwidth [XHG11, TA12]. In addition, studies on AWGs for VLC links based on FPGA have been carried out which also focus on the Media Access Control (MAC) layer [SZC17]. Finally, with achievable sampling rate in the order of Msps and available bandwidth in the order of GHz, FPGAs cover all the requirements for a VLC link.

For this dissertation the Altera DE2 board was chosen, for the implementation of the AWG. The transmitted signal is encoded using rectangular pulse amplitude modulation with a non-return-to-zero (NRZ) line code with Manchester encoding (IEEE 802.3). A pseudorandom binary sequence will be generated by the FPGA in a specific frequency which will represent the data that will be transmitted by the LEDs. This set up will support a RGB LED transmitter, meaning that three different pseudorandom binary sequences, one of each LED, will be developed.

### **2.3.3 Pseudorandom binary sequence**

A pseudorandom binary sequence (PRBS), also known as pseudorandom binary code or pseudorandom bitstream is a binary sequence that is generated by a deterministic algorithm. Particularly, PRBS generators are used in a wide variety of applications, such as telecommunications, cryptography, and statistics. In addition, the repeatability of the sequence depends on the length of the PRBS with the most common example the sequence generated by a linear feedback shift register (LFSR). A typical implementation of a 7-stage LFSR is shown in the Figure 2.5 consisting of a D flip-flop based shift register and a XOR gate in the feedback path.

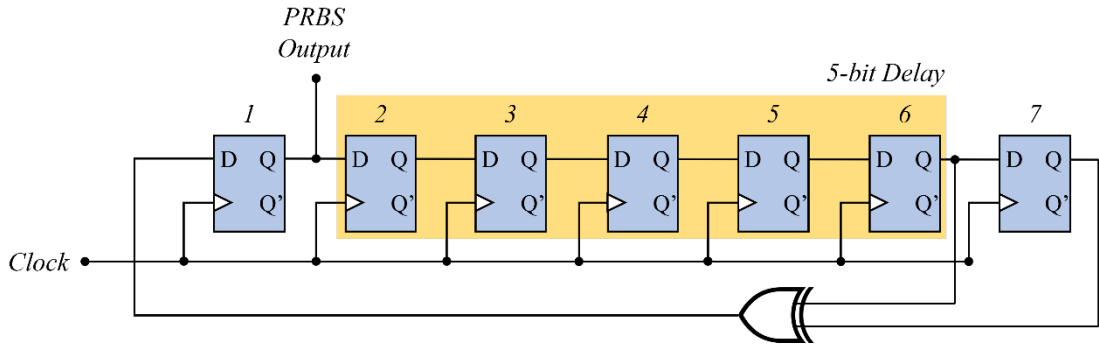


Figure 2.5: A 7-stage LFSR based on D flip-flops and an XOR gate.

The length of the PRBS pattern is determined by the number of the shift registers. For instance, the Table 2.1 shows the length of sequence in bits based on the order of the PRBS. Furthermore, the PRBS can be described by polynomials as shown above in Table 2.2. The exponents from the various PRBS polynomials shown in Table 2.2, represent the feedback taps.

Table 2.1: Length of sequence in bits based on the order of the PRBS.

Sequence	Length of Sequence	Length of Sequence (bits)
PRBS4	$2^4 - 1$	15
PRBS5	$2^5 - 1$	31
PRBS6	$2^6 - 1$	63
PRBS9	$2^9 - 1$	511
PRBS15	$2^{15} - 1$	32,767
PRBS23	$2^{23} - 1$	8,388,607
PRBS31	$2^{31} - 1$	2,147,483,647

During the last years various studies have been conducted for high data rates PRBS can provide data rates in the order Gpbs [KPV12]. Furthermore, areas such as low power consumption, footprint miniaturization and shorten of the critical delay

path have been studied [JH20], making the PRBS a very competitive solution even for WiMax or Bluetooth applications [SSMS21]. Finally, the PRBS has been cost effective [PVT06] and easily available solution because they can achieve the above-mentioned standard even when discrete logical components are used [JH20, SSMS21].

Table 2.2: Monic polynomials based on the order of the PRBS.

Sequence	Monic polynomial
PRBS4	$x^4 + x^3 + 1$
PRBS5	$x^5 + x^3 + 1$
PRBS6	$x^6 + x^5 + 1$
PRBS7	$x^7 + x^6 + 1$
PRBS9	$x^9 + x^5 + 1$
PRBS11	$x^{11} + x^9 + 1$
PRBS13	$x^{13} + x^{12} + x^2 + x + 1$
PRBS15	$x^{15} + x^{14} + 1$
PRBS20	$x^{20} + x^3 + 1$
PRBS23	$x^{23} + x^{18} + 1$
PRBS31	$x^{31} + x^{28} + 1$

The RGB transmitter requires three independent bit streams which will emulate its behavior in real world conditions. For this purpose, three different PRBS have been used, one for each color channel. PRBS4, PRBS5 and PRBS6 were used for the Red, Green and Blue Channels respectively, as shown in Figure 2.6.



output of an XOR gate where inputs are the clock and the bit stream, as show in Figure 2.7.



Figure 2.7: Manchester encoding scheme based on an exclusive OR gate.

Table 2.3: Manchester encoding data using XOR gate.

Original Data		Clock		Manchester encoding
0		0		0
	XOR	1		1
	$\oplus$	0	=	1
1		1		0

### 2.3.5 Clock frequency

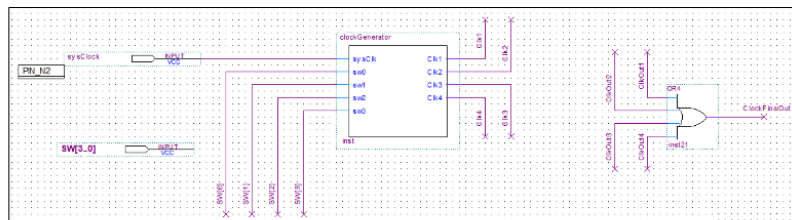
Generating and controlling the proper clock frequency is also an important task which determines the desired operation of both the transmitter circuit and the receiver. In addition, the maximum clock frequency of the Altera DE2 Board is 50 MHz which means that the achievable frequencies must be smaller sub-multiples of this frequency. For this purpose, VHDL code for a counter was developed in order to achieve the desirable frequencies. The count value was calculated as

$$\text{Count Value} = (\text{Input Frequency}) / (2 * \text{Output Frequency}).$$

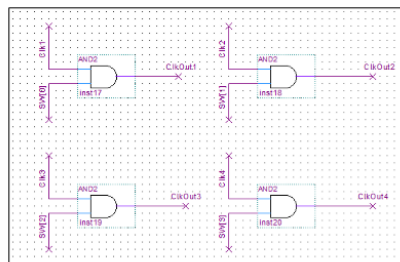
For the completeness of this thesis, it is equally important to examine the VLC link behavior for various clock frequencies. For this reason, three switches of the Altera DE2 Board for choosing among 1.25, 5 and 20 kHz were used

### 2.3.6 Schematic Diagram in Quartus Prime

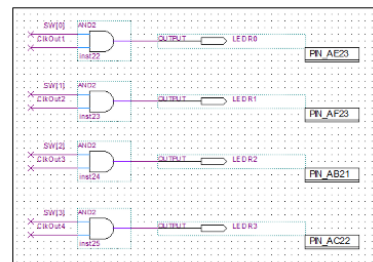
The schematic diagram consists of two parts. The first part involves the clock frequency generator and the second involves the PRBS generator for the three channels as shown in Figures 2.8 and 2.9 respectively. Starting with the clock frequency generator, four switches determine which frequency will be enabled. The second part is controlled by another set of three switches which enable the PRBS4, PRBS5 and PRBS6 respectively. These bit streams carry the data which are transmitted via the RGB LED and through the switches is selected which channel or channels will be enabled. Finally, a final switch is also used to enable one of the board outputs through which the clock can be monitored.



*Clock Frequency Generator*



*Control Switches*



*Altera Red LED Indicators*

Figure 2.8: The clock frequency implementation in the Altera DE2 Board. For different clock frequencies can be selected.

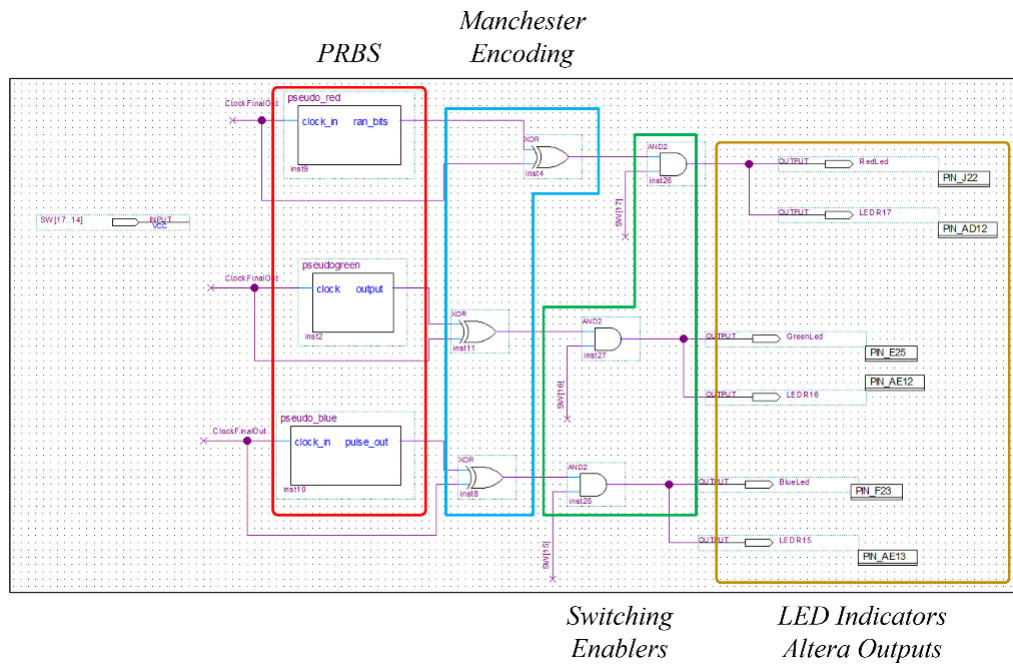


Figure 2.9: The PRBS implementation for the three channels in the Altera DE2 Board.

## 2.4 Experimental Set-up

In this section the experimental set-up is presented and analyzed. In addition, all the stages are analyzed, and the utility of the chosen components is also highlighted. The block diagram of the setup is shown in Figure 2.10 and the experimental set-up is shown in Figure 2.11.

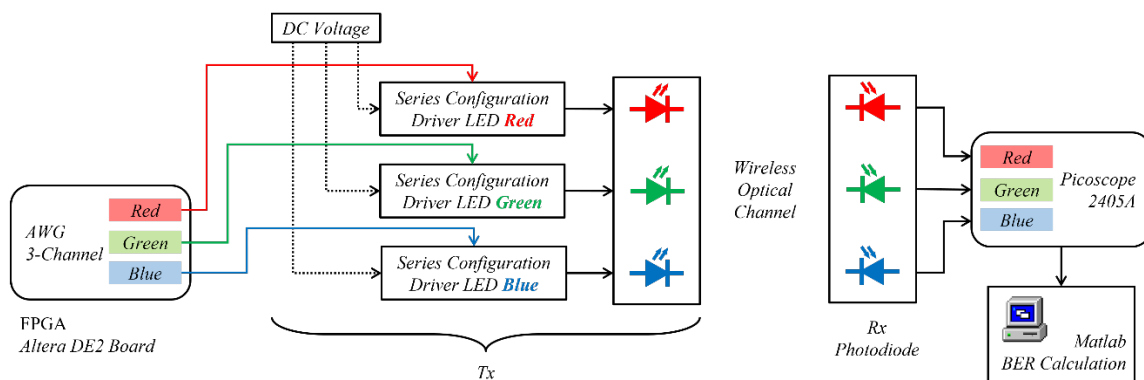


Figure 2.10: Block diagram of the VLC link.

The AWG generates three pseudorandom bitstreams. Each PRBS is applied on the transmitter RGB channels and finally the RGB LED transmits the dedicated signal. The receiver side is composed of the photodiode which receives the signal, which is observed through the through the PicoScope 2405A oscilloscope, the received data are retrieved. Finally, the BER is calculated in Matlab®.

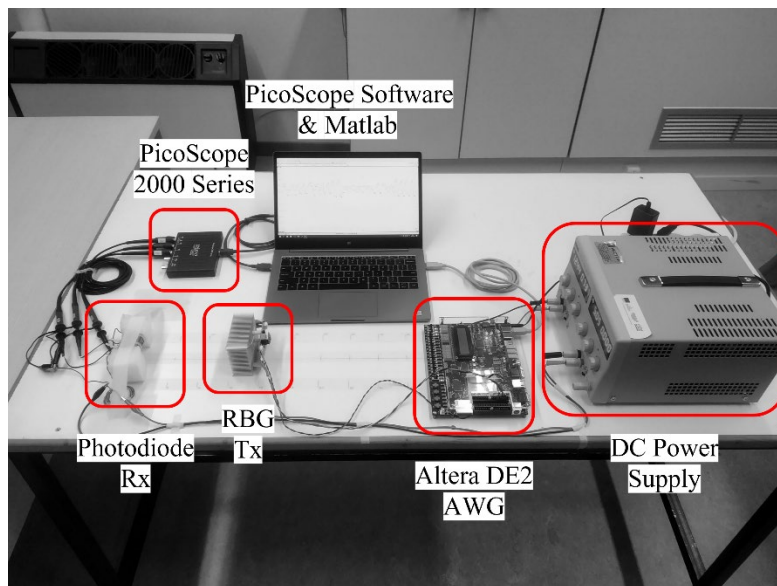


Figure 2.11: The experimental set-up used in the measurements.

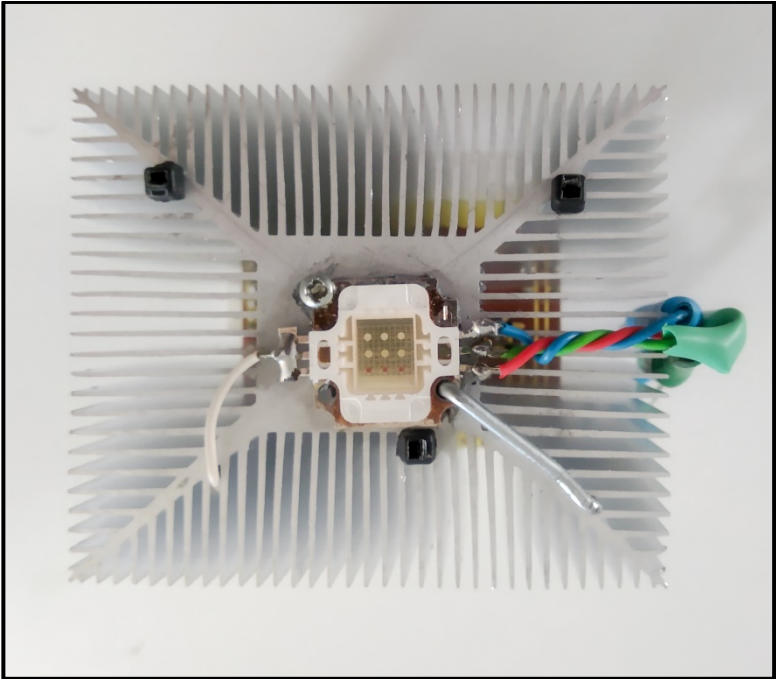
Next the components that have been used are presented:

**TTi EL302 DUAL:** The DC power supplier that provides linear regulated DC with 60 W power supply per output. Moreover, it is equipped with two independent outputs with 4 digits resolution.

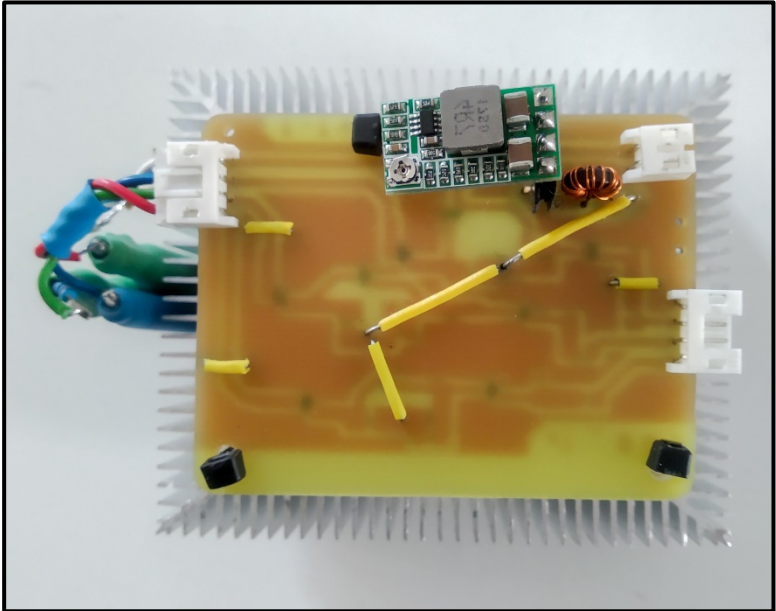
**Altera DE2 Board:** The maximum clock frequency of the FPGA is 50 MHz so that OOK can generated at frequencies that are sub-multiple of this frequency.

**PicoScope 2000 Series – 2405A:** This is a four channel and 25 MHz bandwidth PC USB oscilloscope which is equipped with digital triggering. The maximum sampling rate is at 500 MS/s and the buffer memory at 48 kS.

The RGB LED transmitter and the photodiode receiver are shown in Figure 2.12 and 2.13 respectively.



(a)



(b)

Figure 2.12: The (a) frontage and the (b) backside of the LED RGB transmitter implementation.

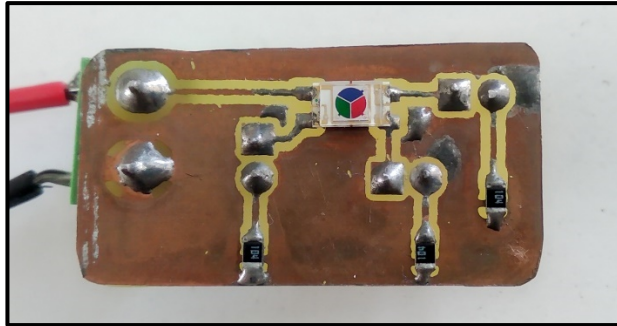


Figure 2.13: The photodiode receiver implementation.

## CHAPTER 3

### CIRCUIT CHARACTERIZATION

---

#### 3.1 Photodiode Characterization

---

#### 3.1 Photodiode Characterization

The photodiode characterization is a very important step for applying the proposed CSK scheme. In the conventional 3-CSK scheme the total intensity of the three LED colors red, green, and blue, is controlled in order to constantly maintain the same lighting performance. Therefore, the three colors intensity measured on the Tx can be expressed as  $P_R$ ,  $P_G$ , and  $P_B$ , for the red, green, and blue LED respectively.

The receiver is equipped with a three-band photodiode (PD) which converts the optical signal into electrical. Furthermore, the band areas are based on the relative spectral responsivity of the PD in comparison with the wavelength. Due to the fact that the band areas overlap with each other, cross-channel interference to the received signals at the photodiode is observed. Figure 3.1 depicts the cross-channel interference during the transmission based on the 3-CSK scheme.

The intensity of the received signals at the PD can be expressed as

$$\begin{bmatrix} P'_R \\ P'_G \\ P'_B \end{bmatrix} = \mathbf{H} \cdot \begin{bmatrix} P_R \\ P_G \\ P_B \end{bmatrix}, \quad (3.1)$$

where  $P'_R$ ,  $P'_G$ , and  $P'_B$  are the intensities of the received signals on the PD from red, green, and blue channel respectively.

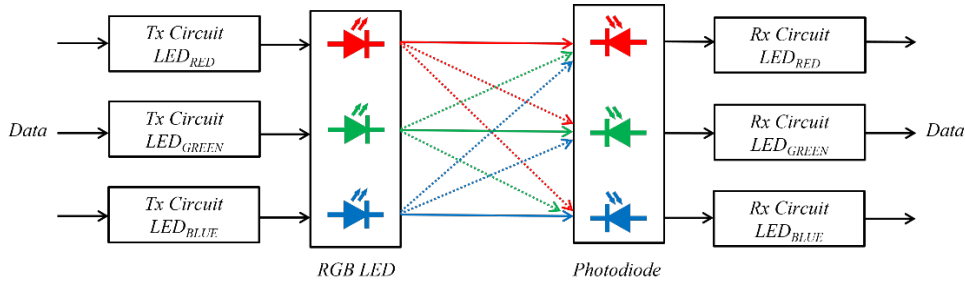


Figure 3.1: The cross-channel interference to received signal from the photodiode. Note that, a single RGB LED is used in the transmitter of this link.

The channel matrix  $\mathbf{H}$  given by

$$\mathbf{H} = \begin{pmatrix} h_{rr} & h_{rg} & h_{rb} \\ h_{gr} & h_{gg} & h_{gb} \\ h_{br} & h_{bg} & h_{bb} \end{pmatrix}, \quad (3.1)$$

where the diagonal entries  $h_{rr}$ ,  $h_{gg}$ , and  $h_{bb}$  are the channel gain between each LED color with the corresponding PD channel and the rest entries represent the crosstalk between channels. Note that, the matrix in Equation 3.1 is asymmetric.

The photodiode response to cross-channel interference creates the concept of the Photodiode Profile. Particularly the photodiode profile was examined in two different cases on the VLC Tx-Rx system discussed in Chapter 2. Firstly, a DC voltage of 12 V with a current of 250 mA was applied directly to the RGB LED and the response of the red, green, and blue photodiode channels was measured. In addition, for this occasion the red, green, and blue LED color combinations were separately examined as shown in Figure 3.2. This process was made in order to compare the actual photocurrent output with the one been presented in the photodiode datasheet. The results are shown in Figure 3.2. Moreover, the inversely proportional effect of the square of the distance on the luminous flux per unit area is shown in Figure 3.3.

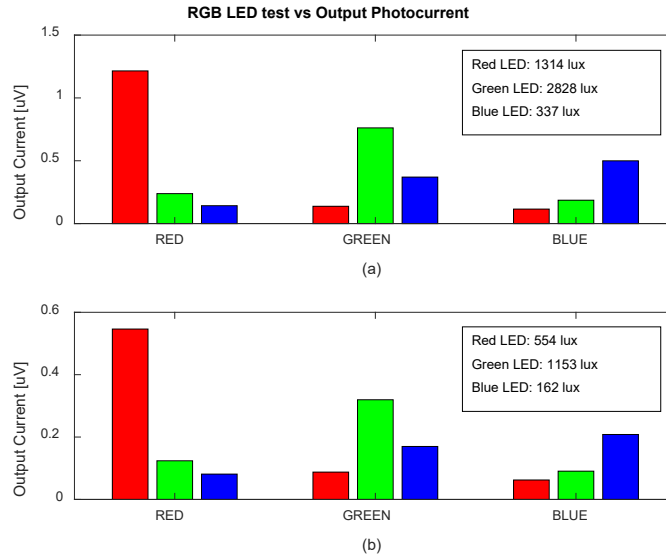


Figure 3.2: The output photocurrent for illuminance of (a) 1943 lx and (b) 840 lx without the presence of the  $R_{LED}$  resistors discussed in Chapter 2.

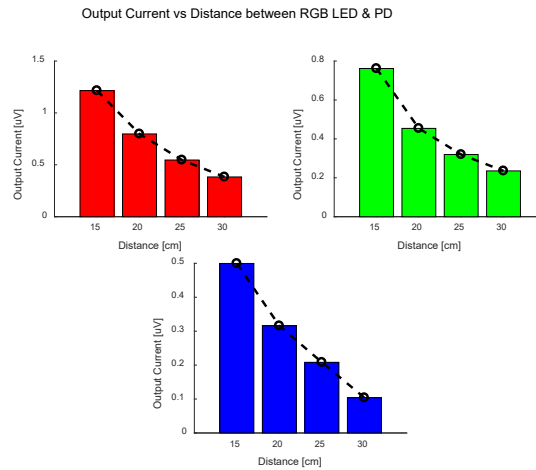


Figure 3.3: The effect of the distance over the measured photocurrent.

For the second case the RGB LED operated based on the lighting standards for indoor applications in the color temperature of 4000 K [IEEEStd]. The resistances ( $R_{LED}$ , see Figure 2.1) that have been used were 42.3  $\Omega$ , 13  $\Omega$  and 62.6  $\Omega$  for the red, green, and blue channels respectively. The presence of the above-mentioned resistances has impact to the photodiode profile and as a result needs to be examined. The photodiode profile for this case is shown in Figure 3.4. When using three different LED colors, eight possible combinations will come up. Furthermore, the performance of the photodiode for these combinations will set the base for the data

retrieval which is presented in Chapter 4. Figure 3.5 shows the performance of each photodiode channel for the eight possible combinations.

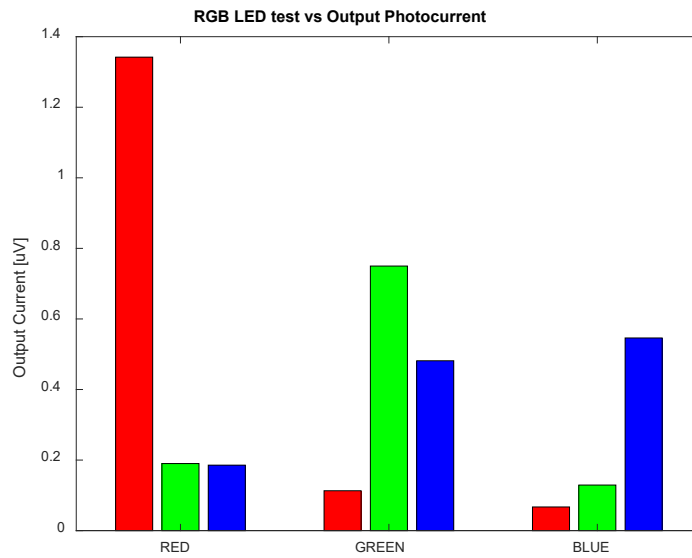


Figure 3.4: The output photocurrent for illuminance of 1943 lx at 4000 K RGB LED operation.

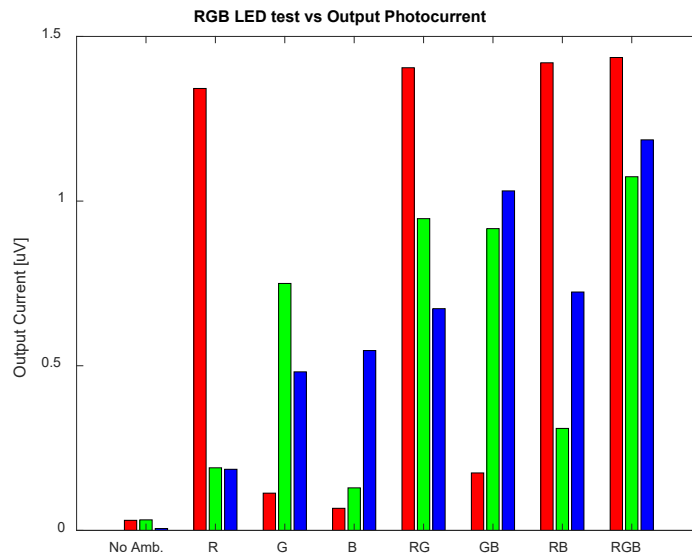


Figure 3.5: The output photocurrent for illuminance of 1943 lx at 4000 K RGB LED operation for the eight possible states. The first state is when no ambient light was applied.

## CHAPTER 4

### DATA RETRIEVAL AT THE RECEIVER

- 
- 4.1 The Data Retrieval Scheme Structure
  - 4.2 Voltage Normalization
  - 4.3 Quantization Error Correction
  - 4.4 Digitization
  - 4.5 Pattern Search
- 

One of the most important advantages of VLC is the use of the color domain to transmit data. To be effective this strategy must be used with light sources that combine several LEDs, such as a red, green, and blue. Particularly, when the LEDs are used for space lighting, it is necessary to maintain the white light, or the color shifts must be indiscernible. In this chapter the data retrieval process at the receiver will be presented. The steps of the proposed scheme can be categorized into five main areas. The area of *Voltage Normalization*, *Quantization Error Correction*, *Digitization*, *Pattern Search* and finally the *Bit Error Rate (BER) Calculation* which is analyzed in Chapter 5. The proposed scheme was designed to characterize the VLC link in the Physical Layer and also to prove whether the method based on the Euclidean distance is applicable or not. However, this scheme is exploited for the link characterization and it is not targeting real-time applications.

## 4.1 The Data Retrieval Scheme Structure

The received data from the three photodiode channels are extracted through the PicoScope 2000 Series, 2405A and processed in Matlab® environment. Furthermore, the three waveforms were saved in a \*.mat file as tables and each table consists of the captured samples. The main principle behind the Data Retrieval Scheme is to extract one sample per half period from each of the three waveforms (red, green, and blue channels) and try to compare them with the states of the photodiode profile and convert them into bits [ManAt, VK17]. Figure 4.1 shows the flowchart of the Data Retrieval Scheme.

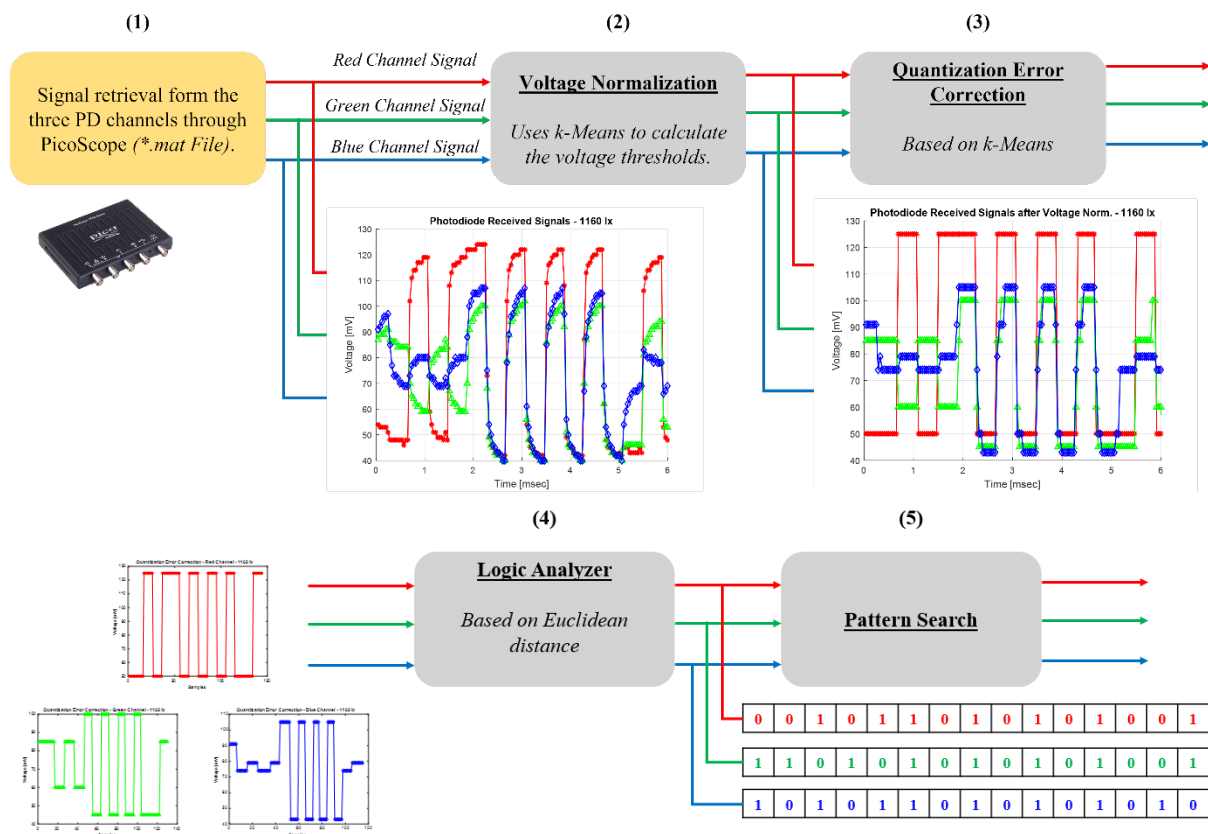


Figure 4.1: Flowchart of the data retrieve scheme.

Whenever data was about to be extracted from PicoScope, the photodiode profile was first measured and then the proposed scheme was applied. For applications where the distance between the transmitter and the receiver was fixed the received

waveforms were characterized by a specific amount of voltage thresholds. In addition, the number of thresholds was not the same for the three channels. The Voltage Normalization stage calculates the thresholds based on the K-Means clustering algorithm. Due to the fact that quantization errors may occur, the second stage tries to correct them. Next, one sample per half period can be extracted and the Logic Analyzer stage can convert the extracted half period samples from the three waveforms into bits. Finally, the Pattern Search stage can be applied in order to calculate the BER and characterize the link.

## 4.2 Voltage Normalization

The Voltage Normalization is based on the K-Means clustering algorithm. The next important question to answer is to determine the number of the groups which will lead to the calculation of the centroids. In addition, the centroids will be the desired thresholds. For this reason, the Elbow Curve method was used. Moreover, this method runs the K-Means clustering from a range of values of  $k$  and for each run the sum of squared distances is calculated. Next through the plot of the average distance from centroids with the corresponding value of  $k$  the “elbow” is revealed. The K-Means algorithm is shown in Algorithm 4.1.

---

### Algorithm 4.1 K-Means

---

- 1: Input:  $D = (d_1, d_2, \dots, d_n)$  // dataset  
 $k$  // the numbers of clusters
  - 2:  $C = (c_1, c_2, \dots, c_k) \leftarrow \text{RandomlySelect}(\{d_1, d_2, \dots, d_k\}, k)$  // centroids
  - 3: **repeat** until assignments  $G_i$  convergence
  - 4:  $G_i \leftarrow \{d: \|d - c_i\|^2 \leq \|d - c_j\|^2 \forall j, 1 \leq i, j \leq k\}$
  - 5:  $c_i \leftarrow \frac{1}{|G_i|} \sum_{c_n \in G_i} d_n$
  - 6: **end repeat**
  - 7: **return**  $C$
-

For each of the three channels the Elbow method was applied, and the results are shown in the Figures 4.2-4.4. For the red channel two clusters needed while for the green and blue six clusters needed.

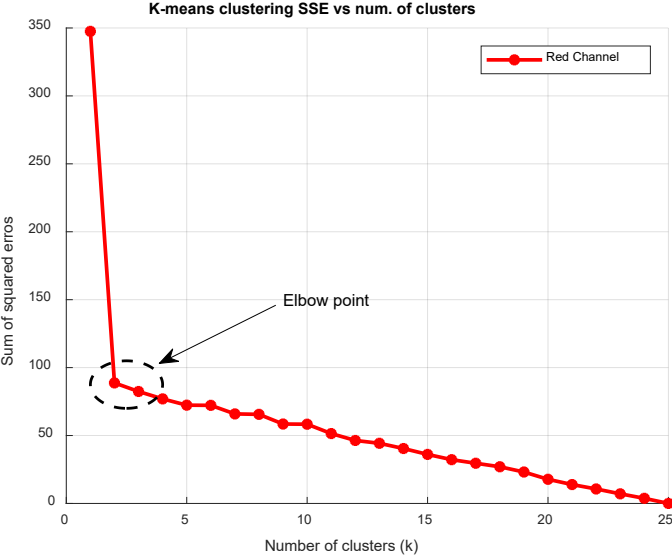


Figure 4.2: The elbow point for the red channel indicates two clusters.

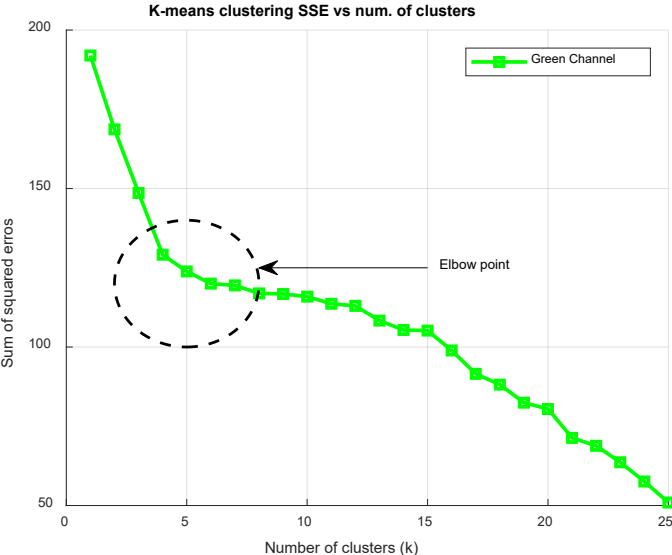


Figure 4.3: The elbow point for the green channel indicates four clusters. The proposed scheme was examined for four, five and six clusters for the green channel, however when used four or five clusters the scheme failed.

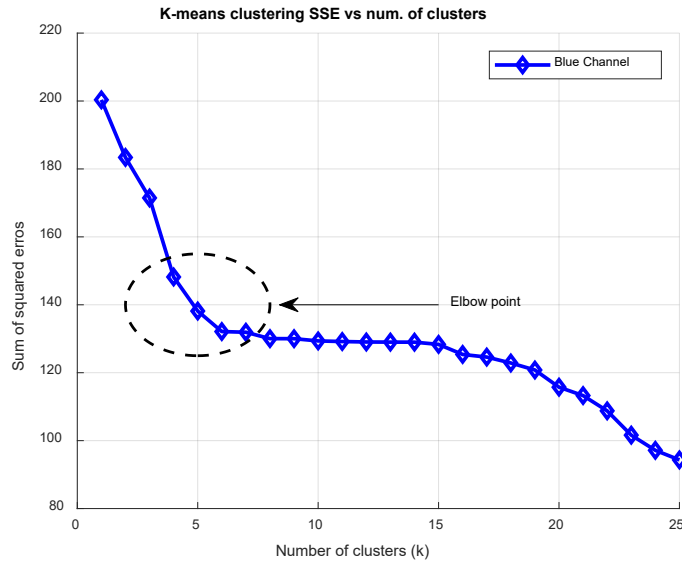


Figure 4.4: The elbow point for the blue channel indicates six clusters.

### 4.3 Quantization Error Correction

In this stage the signal is normalized based on the calculated thresholds from the previous section. In addition, the normalized samples of the red, green, and blue LED signals are stored in three different 1-D matrixes. During the access of each of the three 1-D matrixes, the length of the consecutive identical samples is measured and stored in a new matrix as shown in Figure 4.5.

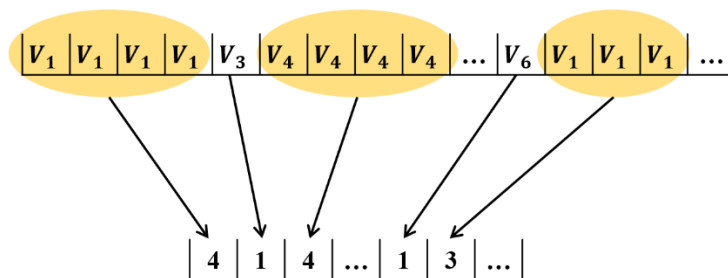


Figure 4.5: The matrix which contains the length of consecutive identical samples.

The length of consecutive identical samples reveals whether they represent a pulse width of one period or half period and also whether it is a quantization error.

Particularly, the length of the consecutive identical samples for a pulse width of one period is almost twice as of the half period case. In addition, the quantization error samples tend to have significant smaller length in comparison with the samples which depict a half period pulse width.

The above-mentioned three case are clustered in groups by using the K-Means algorithm with  $k = 3$ . The consecutive identical samples which belong to the group with the quantization error are removed from the matrix. In addition, if consecutive identical samples belong to the group for the half period pulse width, then only one sample is kept, and the rest are removed. Furthermore, for the one period pulse width case, two samples are kept, and the rest are removed. The same process is applied for all the photodiode channels. Finally, one sample has been extracted every half period for every channel.

#### 4.4 Digitization

At this point one sample for the red, green, and blue PD channels has been retrieved for every half period. The samples are stored in three different matrixes as shown in Figure 4.6. In addition, a point in the Cartesian plane results with coordinates the above-mentioned retrieved samples for every half period. This point can be expressed as  $c_{r,g,b}^j(\text{Sample}R_j, \text{Sample}G_j, \text{Sample}B_j)$  which represents the  $j^{\text{th}}$  bit that is about to be retrieved.

$$\begin{aligned}
 \text{Red}_{\text{Matrix}} &= [\text{Sample}R_0 \ \text{Sample}R_1 \ \dots \ \text{Sample}R_n] \\
 \text{Green}_{\text{Matrix}} &= [\text{Sample}G_0 \ \text{Sample}G_1 \ \dots \ \text{Sample}G_n] \\
 \text{Blue}_{\text{Matrix}} &= [\text{Sample}B_0 \ \text{Sample}B_1 \ \dots \ \text{Sample}B_n]
 \end{aligned}$$

$c_{r,g,b}$

Figure 4.6: Retrieved samples from the PD channels for every half period.

As mentioned in Chapter 3, the photodiode profile is characterized by the eight possible states. In addition, the  $i^{\text{th}}$  photodiode state can be expressed as a point in the Cartesian plane and can be presented as  $s_{r,g,b}^i$ . At this point, it is necessary to

mention that the distance between the Tx and the Rx is fixed and the corresponding photodiode profile has been retrieved.

The signal digitization is done by calculating the Euclidean distance between each half period color sample with the eight photodiode states [NFV15]. The Euclidean distance between the  $j^{th}$  received color sample  $c$  with the  $i^{th}$  photodiode state is given by

$$d_{r,g,b}^i = \sqrt{(s_r^i - c_r^j)^2 + (s_g^i - c_g^j)^2 + (s_b^i - c_b^j)^2}. \quad (4.1)$$

In order to choose the closest possible state, all the distances between the other seven states with the received color sample must be calculated. The chosen state would be

$$\min(d_{r,g,b}^0, \dots, d_{r,g,b}^i, \dots, d_{r,g,b}^7). \quad (4.2)$$

In case the minimum distance between the received color sample with the photodiode states is equal to more than one states, then the state is chosen randomly among them. Finally, each state indicates whether which of the red, green, and blue LEDs are switched on or off and as a result the binary bits are retrieved. Figure 4.7 shows the Euclidean distance between the received color sample with the photodiode states.

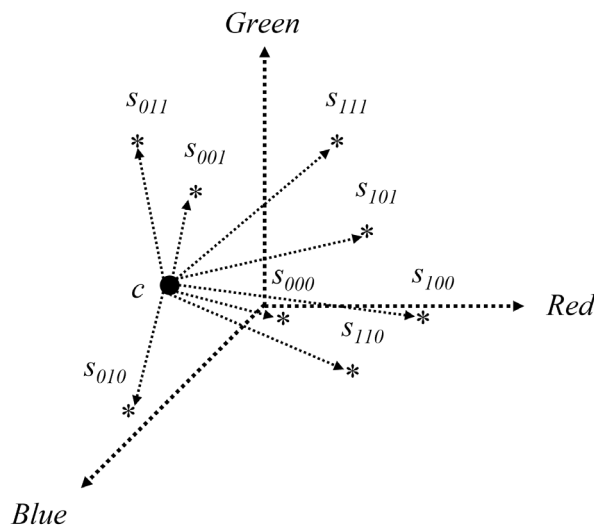


Figure 4.7: Euclidean distance between the received color  $c$  and the eight different possible states.

## 4.5 Pattern Search

The Pattern Search step receives the digitized signal and stores every  $k$  digits in a different line of a 2-D matrix where  $k$  is the length of the PRBS. The 2-D matrix consists of  $\lceil m/k \rceil$  lines, where  $m$  is the length of the retrieved bits. The first approach is to propose a pattern which calculates the most frequent value of each column of the 2-D matrix. The block diagram for this process is shown in Figure 4.8.

If the proposed pattern fails to match with the PRBS then an alternative approach is applied. Each line of the 2-D matrix is compared separately with the PRBS. The scheme is applied as follows:

1. The PRBS rotates until as many values as possible match with those of the compared line of the 2-D matrix in the corresponding positions.
2. The number of the applied rotations is stored.
3. The same process is applied for all the lines of the 2-D matrix.
4. The pattern is found if the same rotation value is applied for the majority of the lines.

For this method a special case may arise. For instance, if the matching rate of a line is the same for more than one rotation values then this line is not taken into consideration. The block diagram for the alternative pattern retrieve method is shown in Figure 4.9.

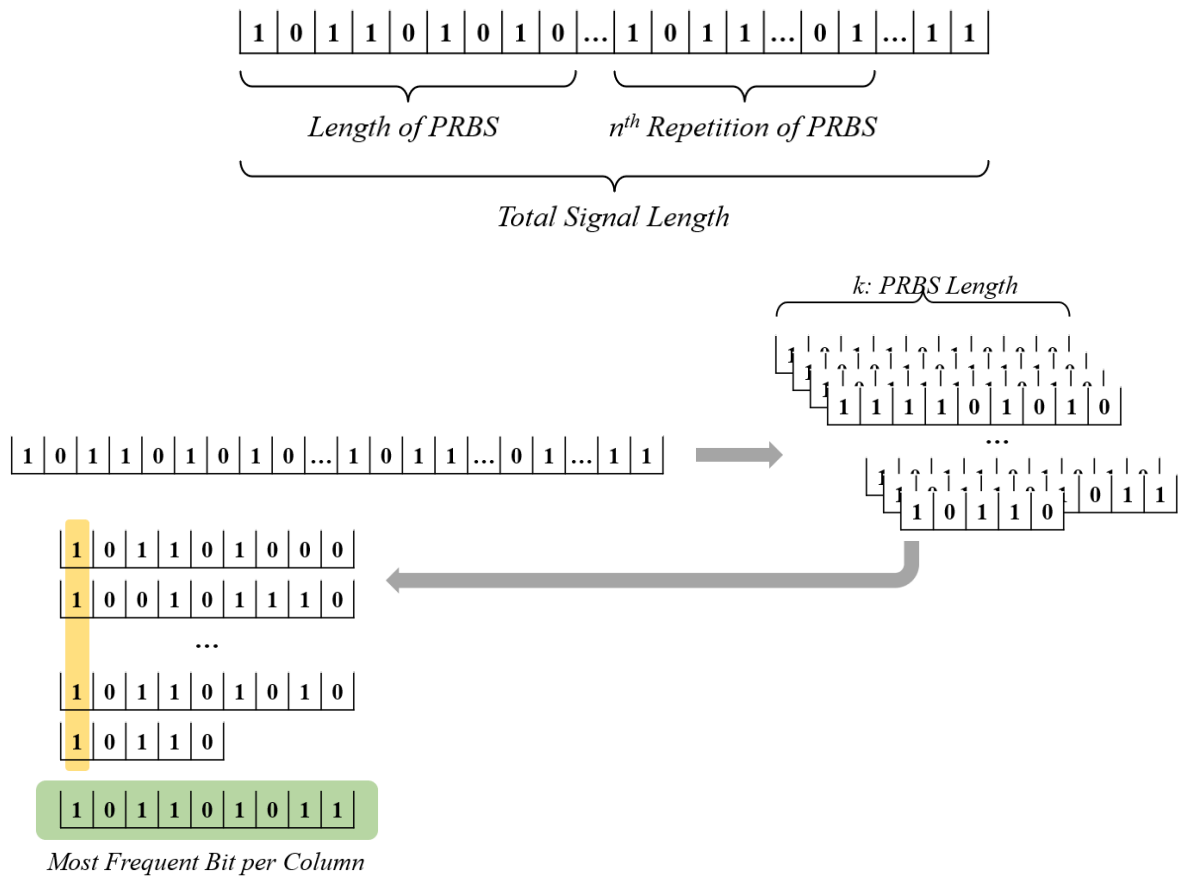


Figure 4.8: Block diagram of the Pattern Search stage for the first attempt to retrieve the PRBS pattern.

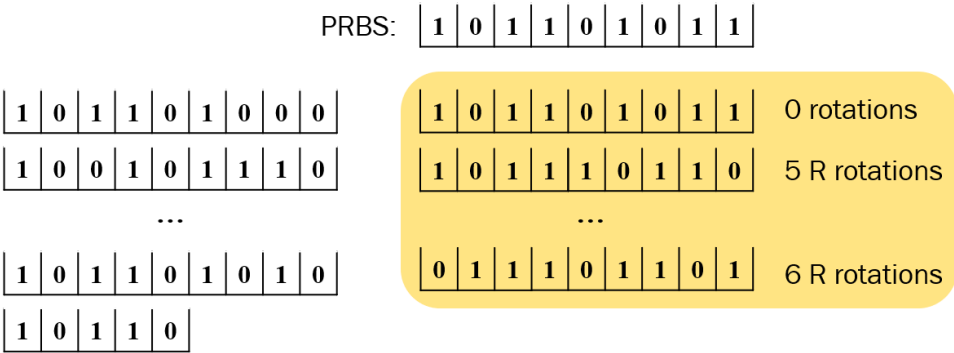


Figure 4.9: Block diagram of the Pattern Search stage for the alternative method to retrieve the PRBS pattern.

# CHAPTER 5

## RESULTS

---

### 5.1 Effect of the Illuminance to SNR

### 5.2 BER Analysis

---

### 5.1 Effect of the Illuminance to SNR

The experimental results in this section were taken in an environment where ambient or any source of artificial light were off during the evening hours. The reason those conditions were chosen was to avoid the interference of noise from the environment. In this section the effect of the illuminance to Signal-to-Noise ratio (SNR) is examined. The SNR based on signal and noise voltages is calculated as follows

$$SNR_{dB} = 20 \cdot \log\left(\frac{S_V}{N_V}\right), \quad (5.1)$$

where  $S_V$ ,  $N_V$  are the signal and noise voltage respectively. In addition, the instantaneous noise amplitude is within  $\pm 3\sigma$  of the mean 99.7% of the time as shown in Figure 5.1 [BC9]. The examined frequencies for the three channels, red, green, and blue, were 1.25, 5 and 20 kHz. In Figures 5.2-5.4, the impact of the illuminance to the Signal-to-Noise ratio (SNR) is presented for the above-mentioned frequencies.

The first observation from the Figures 5.2-5.4 is the logarithmic increase of the SNR with the illuminance increase. This is due to the dependence of the surface

illumination on the distance from the source as shown in Chapter 1. In other words, this increase of BER is due to the fact that the photocurrent is inversely proportional to the distance it has from the source. Furthermore, based on the indoor lighting standards [IEEEStd] the intended illuminance must be around 500 lx. The calculated SNR for this area is very low and this due to the fact that no amplifiers have been added to the receiver in this study.

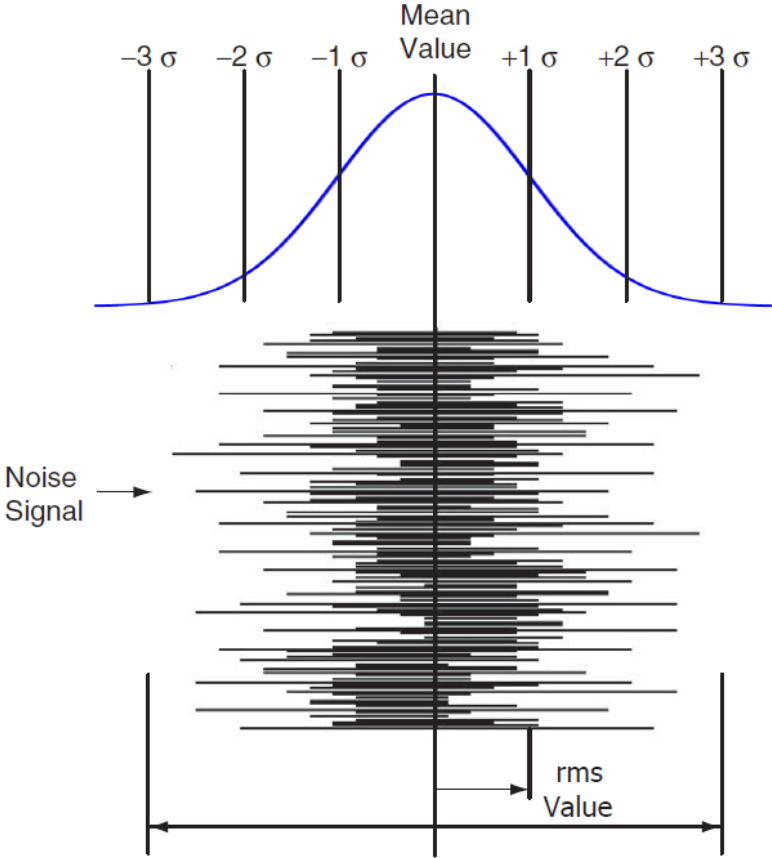


Figure 5.1: Gaussian distribution of noise energy<sup>2</sup>.

Another observation is that the red channel shows the best performance while the blue channel the worst. This is due to the sensitivity of the photodiode, as indicated in the datasheet, but also to the fact that the temperature of the RGB LED was 4000 K. In order to achieve this color temperature, the illuminance of the blue

---

<sup>2</sup> Reprinted from Bruce Carter, Chapter 12 - Op Amp Noise Theory and Applications, Editor(s): Ron Mancini, Bruce Carter, Op Amps for Everyone (Third Edition), Newnes, 2009, Pages 163-188, ISBN 9781856175050, <https://doi.org/10.1016/B978-1-85617-505-0.00012-0>.

channel had to be reduced enough, as can be seen from the selection of the resistor in Chapter 3.

The increase of the frequency has also impact on the SNR. Particularly, increasing the frequency the photodiode does not have time to raise the voltage so that the received signal is altered and cannot reach its peak. As a consequence, the total signal power reduces as it can be seen in Figures 5.2-5.4.

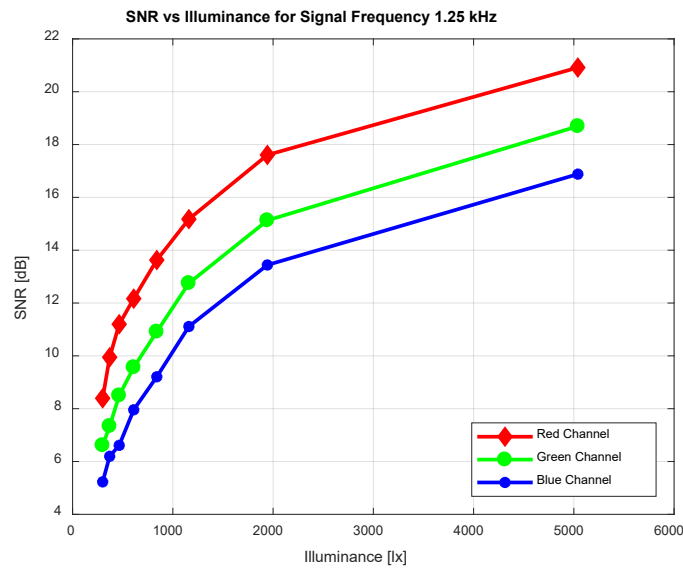


Figure 5.2: Curves of SNR versus illuminance for signal frequency 1.25 kHz.

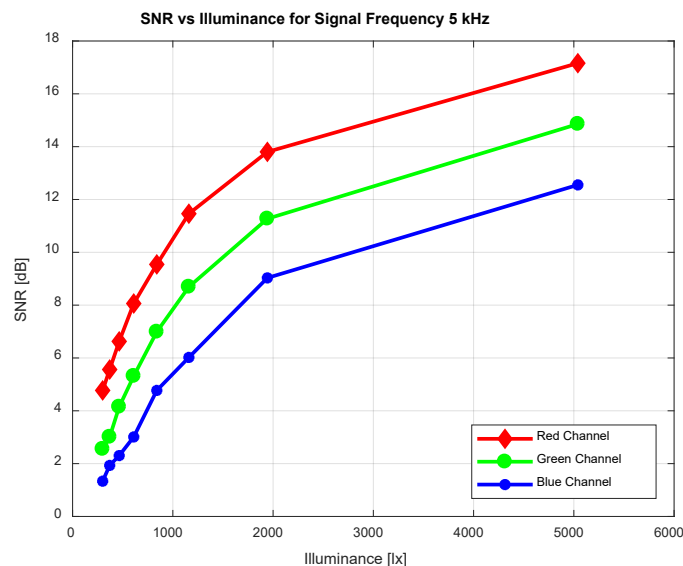


Figure 5.3: Curves of SNR versus illuminance for signal frequency 5 kHz.

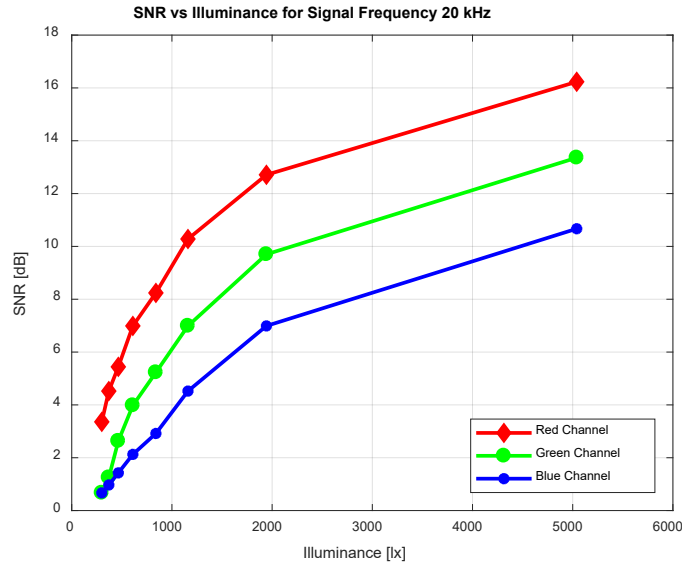


Figure 5.4: Curves of SNR versus illuminance for signal frequency 20 kHz.

## 5.2 BER Analysis

In this section the BER for the VLC link will be examined. Firstly, for reasons of completeness of this work, it was decided to calculate the BER for each channel separately. The BER is calculated by the Equation 5.2.

$$BER = \frac{Errors}{Total\ Number\ of\ Bits} \quad (5.2)$$

As seen from the Figure 5.5-5.7 the red channel shows the best performance while the blue the worse. Furthermore, the SNR and the BER are closely linked and as a result the lower illuminance of the blue channel gave a negative impact to the blue channel BER. Note once again that the photodiode receiver is not equipped with amplifiers and as a result the processed signal is very low.

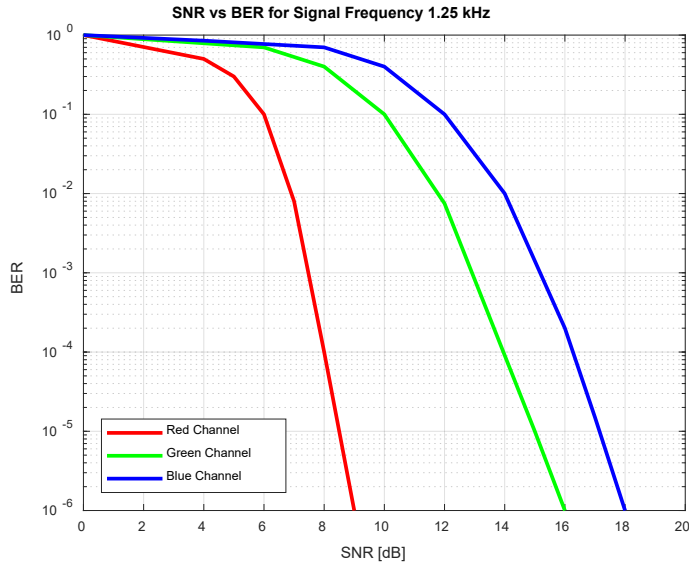


Figure 5.5: Curves of SNR versus BER for signal frequency 1.25 kHz.

The impact of the frequency on the BER is also shown by the Figures 5.5-5.7 and as the frequency increases the BER is getting worse. Furthermore, the performance of the green and the blue is comparable while the red shows a big lead. This is due to the reasons explained in the previous section regarding the sensitivity of the photodiode and the choice of color temperature.

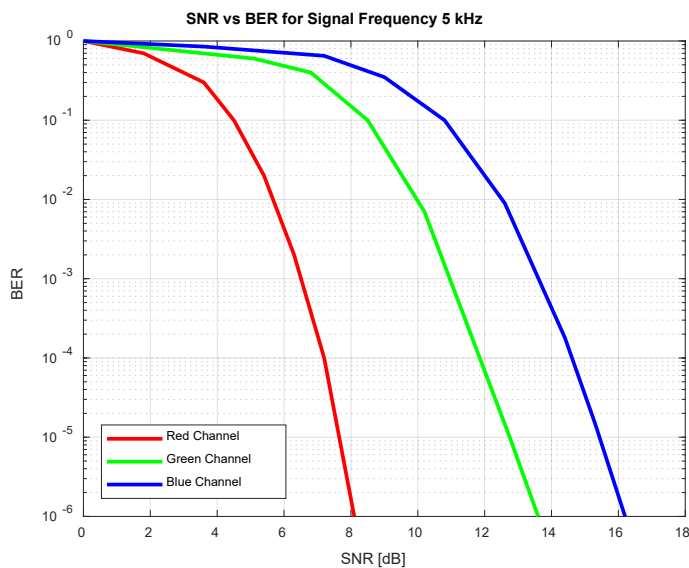


Figure 5.6: Curves of SNR versus BER for signal frequency 5 kHz.

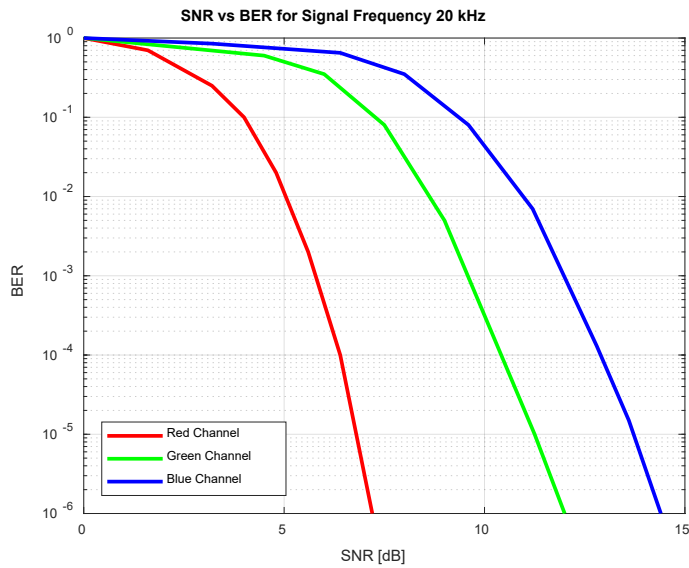


Figure 5.7: Curves of SNR versus BER for signal frequency 20 kHz.

The impact of the frequency on the signal voltage swing and the distortions it causes are shown in the Figures 5.8 and 5.9. Furthermore, by increasing the frequency from 1.25 kHz to 20 kHz the electrical power of the red channel decreased almost 20%, also 30% and 40% for the green and blue respectively.

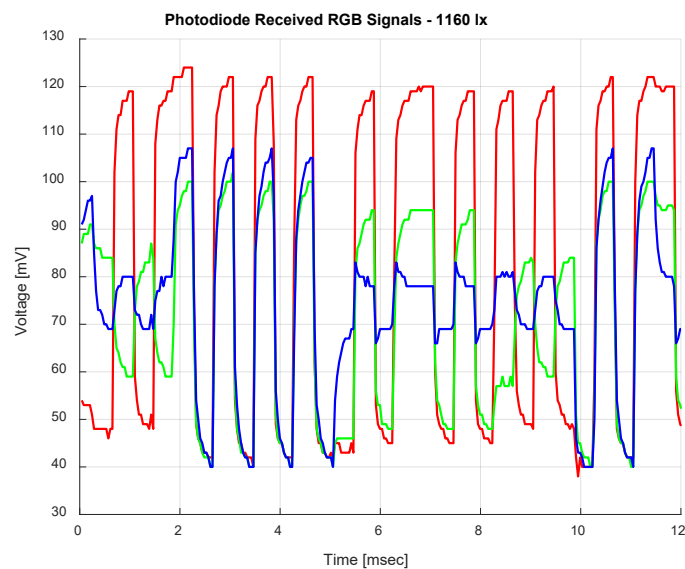


Figure 5.8: A 1.25 kHz received signal.

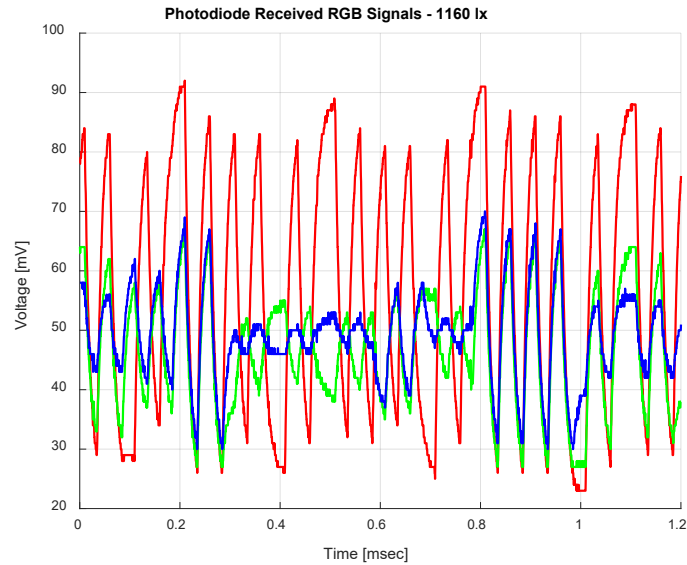


Figure 5.9: A 20 kHz received signal.

Figure 5.10 shows the correlation between of the illuminance and the total BER. The total BER is calculated by the total number of errors from all the three channels divided by the total number of the transmitted bits from all the three channels. When the clock frequency is 1.25 kHz, the total BER around the 500 lx is  $10^{-4} - 10^{-3}$ . This BER value is not the optimal, however the margin for further improvement is big. Moreover, even though for 5 and 20 kHz the BER is around  $10^{-2}$  and  $10^{-1}$  there is also the margin for improvement by amplifying the signals at the receiver.

The effect of the distance to the total BER is shown in Figure 5.11. Again, the lower frequencies operate better in comparison with the higher. Furthermore, it is shown that the upper limit for our test set-up is the distance of 40 cm or the illuminance of 370 lx. In addition, for the clock frequency of 1.25 kHz the range where the lowest total BER is  $10^{-6}$  is x1.25 and x1.67 larger in comparison the 5 and 20 kHz clock frequencies respectively.

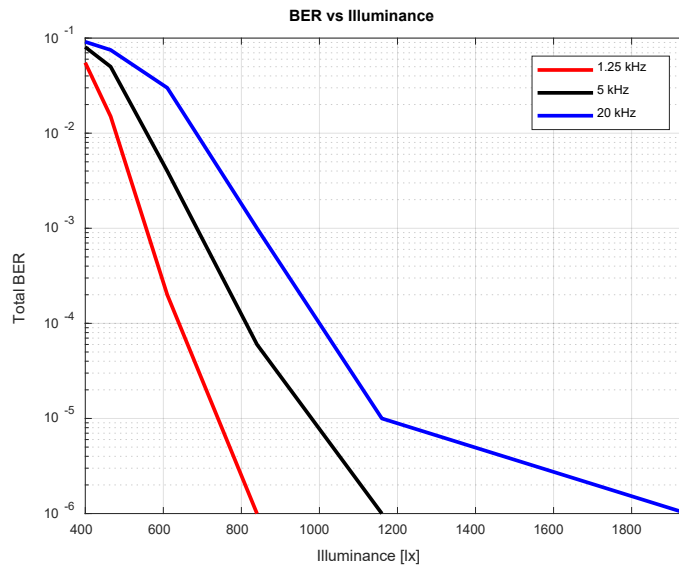


Figure 5.10: Curves of illuminance versus BER for signal frequencies 1.25, 5 and 20 kHz.

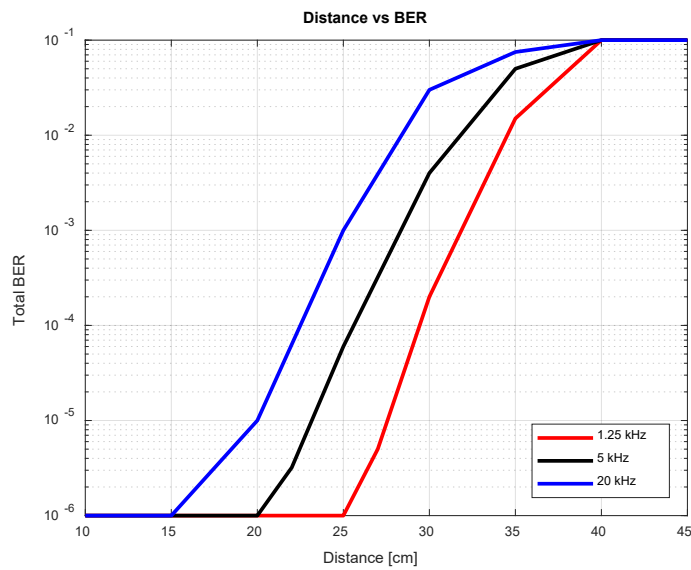


Figure 5.11: Curves of distance versus BER for signal frequencies 1.25, 5 and 20 kHz.

## CHAPTER 6

# CONCLUSIONS AND FUTURE WORK

---

### 6.1 Conclusions

### 6.2 Future Work

---

## 6.1 Conclusions

This work focused on the development of a VLC link based on a 3-CSK scheme for indoor applications. Moreover, the thesis could be categorized in two large groups: a) the hardware-oriented and b) the software-oriented implementations. The hardware-oriented implementations are focused on the design and construction of the VLC link. In addition, the software-oriented implementations were focused on the received signal at the photodiode. Both implementations are discussed briefly in the next paragraph.

The first part was the design and the construction of the RGB LED transmitter and the photodiode receiver which were the most important hardware implementations for the VLC link. Next, for the implementation of a pseudorandom binary sequence generator that is required for the link evaluation, a FPGA platform was used. The second part was dedicated to the signal retrieval from the three channels of the photodiode. For the BER calculation the K-Means clustering algorithm was used along with the proposed scheme. In addition, the proposed scheme used the Euclidean distance for the digitization of the received signal. Finally, the link was characterized based on the calculated BER, and SNR with respect to the illuminance.

Designing and implementing robust links which will present tolerance to BER while keeping the cost at low levels, is a very challenging task for the modern telecommunication networks. This task becomes more difficult when the designer has to deal the limited bandwidth and the electromagnetic interference. For these reasons, VLC links tend to be a solid, sustainable, and easily applicable solution which will operate as an auxiliary for the telecommunication networks.

The components that have been used were carefully selected to fulfill the above-mentioned requirements and to be easily adapted to the existing lighting infrastructure for minimizing the cost. Furthermore, the proposed CSK scheme can be easily applicable and with some extra modifications to the receiver, the VLC link will be capable to achieve acceptable performance levels.

OWC has been for many years an open research topic with great prospects but with no practical use for commercial applications. Over the last years, the technology of photodiodes along with the rise of optical networks and photonics due to their high bandwidth, have brought the OWC in the foreground. Furthermore, the ability to combine the worlds of electronics with the optical domain have set new capabilities and possibilities to the tomorrow's networks. So, will the OWC be the main wireless network technology in the future?

## 6.2 Future Work

Although the proposed 3-CSK was used to characterize the photodiode channels the need for increased bandwidth along with better BER performance is imperative. Towards this direction, the use of signal amplifiers at the receiver side along with the exploitation of dichroic filters should be examined. The combination of these two issues might unlock the true capabilities of the RGB VLC link. The addition of the amplifiers is a crucial step which is the first that should be done. Furthermore, dichroic filters might better separate the channels and as a result contribute positively to the cross-channel interference reduction.

Another challenging issue is the use of a CSK scheme with more than three colors. Although, the complexity of the optical channel will be increased, the advantages with respect to the available bandwidth will also increase.

The performance of the 3-CSK on real-time applications or devices with low computational power, such as IoT devices, is also another area for further investigation. Another equally important study would be the examination of different modulation formats which utilize better the available bandwidth.

Finally, for applications with the presence of many transmitters in the same area new problems must be examined. For instance, graph problems, handover policies for moving users, overlapping areas, security issues are some of the topics of great interest.

## BIBLIOGRAPHY

---

- [LYW17] X. Liang, M. Yuan, J. Wang, Z. Ding, M. Jiang and C. Zhao, "Constellation Design Enhancement for Color-Shift Keying Modulation of Quadri-chromatic LEDs in Visible Light Communications," in *Journal of Lightwave Technology*, vol. 35, no. 17, pp. 3650-3663, 1 Sept.1, 2017, doi: 10.1109/JLT.2017.2720579.
- [PW20] A. Pepe, Z. Wei, and H. Fu, "Heuristic, machine learning approach to 8-CSK decision regions in RGB-LED visible light communication," *OSA Continuum* 3, 473-482 (2020).
- [SK15] H. Shimamoto, Y. Kozawa and Y. Umeda, "An experimental evaluation on EVM performance for 4-CSK(Color Shift Keying) using visible light with multiple full-color LEDs," 2015 IEEE Radio and Wireless Symposium (RWS), 2015, pp. 206-208, doi: 10.1109/RWS.2015.7129740.
- [PVT06] L. Pavlovic, M. Vidmar and S. Tomazic, "2.5 Gbit/s PRBS Generator and Checker," *Proceedings ELMAR 2006*, 2006, pp. 363-366, doi: 10.1109/ELMAR.2006.329585.
- [KPV12] V. Kozlov, P. Park and S. P. Voinigescu, " $4 \times 24$  Gb/s  $2^7 - 1$  PRBS generator using 1.8 V MOS-HBT Quasi-CML logic," 2012 IEEE Bipolar/BiCMOS Circuits and Technology Meeting (BCTM), 2012, pp. 1-4, doi: 10.1109/BCTM.2012.6352614.
- [EMW8] Mohamed El-Moghazi, Jason Whalley, and Peter Curwen. *Is refarming the answer to the spectrum shortage conundrum?* 2008.

- [JH20] J. Hu et al., "An 18-Gb/s  $36 \times 13$ - $\mu\text{m}^2$  3.53-mW 27-1 PRBS Generator in 40-nm CMOS," 2020 International Conference on Electronics, Information, and Communication (ICEIC), 2020, pp. 1-2, doi: 10.1109/ICEIC49074.2020.9051329.
- [BB4] Russell W Burns and Russell W Burns. Communications: an international history of the formative years. IET, 2004.
- [SSMS21] M. K. Singh, P. Singh, D. Mrinal Das and M. Sakare, "A low power  $8 \times 27$ -1 PRBS generator using Exclusive-OR gate merged D flip-flops," 2021 IEEE International Midwest Symposium on Circuits and Systems (MWSCAS), 2021, pp. 779-782, doi: 10.1109/MWSCAS47672.2021.9531827.
- [SZC17] Y. Sha, M. Zhang and T. Cheng, "A research of media access control for indoor VLC LAN based on FPGA," 2017 16th International Conference on Optical Communications and Networks (ICOON), 2017, pp. 1-3, doi: 10.1109/ICOON.2017.8121357.
- [IEEEstd] "IEEE Standard for Local and metropolitan area networks--Part 15.7: Short-Range Optical Wireless Communications," in IEEE Std 802.15.7-2018 (Revision of IEEE Std 802.15.7-2011) , vol., no., pp.1-407, 23 April 2019, doi: 10.1109/IEEEESTD.2019.8697198.
- [KV21] Verniers, Kevin. Investigation of Visible Light Communication in a Realistic Indoor Illumination Scenario. 2021.
- [UCG16] Murat Uysal, Carlo Capsoni, Zabih Ghassemlooy, Anthony Boucouvalas, and Eszter Udvary. Optical wireless communications: an emerging technology. Springer, 2016.
- [HH15] Harald Haas. Visible light communication. In 2015 Optical Fiber Communications Conference and Exhibition (OFC), pages 1–72. IEEE, 2015.
- [NFV15] Ndjiongue, Alain Richard & Ferreira, Hendrik & Vinck, A.J. Han. (2015). Segmental Analysis of the Transmission in CSK Systems Based on the Euclidean Distance. 10.13140/RG.2.1.5176.1124.

- [PFHM15] Parth H Pathak, Xiaotao Feng, Pengfei Hu, and Prasant Mohapatra. Visible light communication, networking, and sensing: A survey, potential and challenges. *IEEE communications surveys & tutorials*, 17(4):2047–2077, 2015.
- [TA12] T. Alpert et al., "Arbitrary Waveform Generator Based on FPGA and High-Speed DAC with Real-Time Interface," *PRIME 2012; 8th Conference on Ph.D. Research in Microelectronics & Electronics*, 2012, pp. 1-4.
- [XHG11] M. Xu, J. Hu and Y. Gao, "FPGA-Based Design and Implementation of Arbitrary Waveform Generator," *2011 International Conference on Control, Automation and Systems Engineering (CASE)*, 2011, pp. 1-4, doi: 10.1109/ICCASE.2011.5997708.
- [ManAt] APPLICATION NOTE, Manchester Coding Basics, MANCHESTER CODING BASICS, Atmel: [http://ww1.microchip.com/downloads/en/APPNotes/Atmel-9164-Manchester-Coding-Basics\\_Application-Note.pdf](http://ww1.microchip.com/downloads/en/APPNotes/Atmel-9164-Manchester-Coding-Basics_Application-Note.pdf)
- [VK17] Vijay Kumar, "Beginners Guide to Clock Data Recovery – PDA", *CDR Basics*
- [BC9] Bruce Carter, Chapter 12 - Op Amp Noise Theory and Applications, Editor(s): Ron Mancini, Bruce Carter, *Op Amps for Everyone (Third Edition)*, Newnes, 2009, Pages 163-188, ISBN 9781856175050, <https://doi.org/10.1016/B978-1-85617-505-0.00012-0>.

## SHORT BIOGRAPHY

---

Georgios Megas obtained his diploma from the School of Electrical and Computer Engineering at the National Technical University of Athens (NTUA), in 2020. His thesis was carried out at the Photonics Communications Research Laboratory (PCRL) focusing on microwave photonics for 5th generation mobile communications.

He has participated in various scientific projects in the areas of photonics, software-defined networking (SDN), cyber-physical systems security and wireless optical communications. He has also worked as a research assistant at the VCAS Lab: VLSI Systems and Computer Architecture Laboratory of the University of Ioannina. His research activities include among other photonics, optical networks, optical wireless communications, electronics.